Atmos. Chem. Phys. Discuss., 13, 8701–8767, 2013
www.atmos-chem-phys-discuss.net/13/8701/2013/
doi:10.5194/acpd-13-8701-2013
© Author(s) 2013. CC Attribution 3.0 License.

Atmospheric Chemistry and Physics Discussions

This discussion paper is/has been under review for the journal Atmospheric Chemistry and Physics (ACP). Please refer to the corresponding final paper in ACP if available.

Laboratory studies of immersion and deposition mode ice nucleation of ozone aged mineral dust particles

Z. A. Kanji[1,*], **A. Welti**[1], **C. Chou**[1,**], **O. Stetzer**[1], **and U. Lohmann**[1]

[1]Institute for Atmospheric and Climate Sciences, ETH, Zurich, 8092, Switzerland
[*]now at: Air Quality Research Division, Environment Canada, Toronto, ON M3H 5T4, Canada
[**]now at: Science and Technology Research Institute, University of Hertfordshire, College Lane, AL10 9AB, Hatfield, UK

Received: 14 March 2013 – Accepted: 21 March 2013 – Published: 2 April 2013

Correspondence to: Z. A. Kanji (zamin.kanji@env.ethz.ch)

Published by Copernicus Publications on behalf of the European Geosciences Union.

Abstract

Ice nucleation in the atmosphere is central to the understanding the microphysical properties of mixed-phase and cirrus clouds. Ambient conditions such as temperature (T) and relative humidity (RH), as well as aerosol properties such as chemical composition and mixing state play an important role in predicting ice formation in the troposphere. Previous field studies have reported the absence of sulphate and organic compounds on mineral dust ice crystal residuals sampled at mountain top stations or aircraft based measurements despite the long range transport mineral dust is subjected to. We present laboratory studies of ice nucleation for immersion and deposition mode on ozone aged mineral dust particles for $233 < T < 263$ K that will represent ageing but not internal mixing with in(organic) compounds. Heterogeneous ice nucleation of untreated kaolinite (Ka) and Arizona Test Dust (ATD) particles is compared to corresponding aged particles that are subjected to ozone exposures of 0.4–4.3 ppmv in a stainless steel aerosol tank. The portable ice nucleation counter (PINC) and immersion chamber combined with the Zurich ice nucleation chamber (IMCA – ZINC) are used to conduct deposition and immersion mode measurements respectively. Ice active fractions as well as ice active surface site densities (n_s) are reported and observed to increase as a function of temperature. We present first results that demonstrate enhancement of the ice nucleation ability of aged mineral dust particles in both the deposition and immersion mode due to ageing. Additionally, these are also the first results to show a suppression of heterogeneous ice nucleation without the condensation of a coating of (in)organic material. In immersion mode, low exposure Ka particles showed enhanced ice activity requiring a median freezing temperature of 1.5 K warmer than that of untreated Ka whereas high exposure ATD particles showed suppressed ice nucleation requiring a median freezing temperature of 3 K colder than that of untreated ATD. In deposition mode, low exposure Ka had ice active fractions of an order of magnitude higher than untreated Ka, where as high exposure ATD had ice active fractions up to a factor of 4 lower than untreated ATD. Based on our results, we present

ACPD
13, 8701–8767, 2013

parameterizations in terms of $n_s(T)$ that can represent ice nucleation of atmospherically aged and non-aged particles for both immersion and deposition mode. We find excellent agreement (to within less than a factor of 2) with field measurements when parameterizations derived from our results are used to predict ice nuclei concentrations in the troposphere.

1 Introduction

Ice crystals form in tropospheric clouds through homogeneous and heterogeneous nucleation mechanisms. Understanding the processes of freezing and the conditions that lead to ice formation is necessary since ice nucleation governs the microphysical properties of ice and mixed-phase clouds whose contribution to the Earth's radiation budget are still uncertain (Denman et al., 2007). Knowledge of the properties of atmospheric particles that change ice nucleation ability of particles is necessary in order to appropriately treat the process in global circulation models and predict ice crystal concentrations in the troposphere. Such information is useful for a number of reasons. First, accurately predicting water vapour mixing ratios requires the quantification of ice particle sizes and numbers in the atmosphere since ice is an important sink of gas phase water, an especially active green-house gas in the upper troposphere (Lindzen, 1990). Second, ice acts as a surface for heterogeneous chemistry through the uptake of many trace gases (Kolb et al., 2010; Abbatt, 2003) for example SO_2 and O_3, thus ice particles in the atmosphere play a crucial role in determining the chemical composition of the troposphere. Third, global precipitation is mostly initiated by the ice phase and thus determining cloud cover and life time are dependent on the amount of ice formed in a mixed-phase cloud (Lohmann and Feichter, 2005).

Heterogeneous ice nucleation where an atmospheric solid particle aids ice crystallization is classified into different modes (Vali, 1985) namely, deposition mode, in which vapour supersaturated with respect to ice deposits onto an aerosol particle surface directly as ice, contact freezing, in which freezing initiates at the interface of contact

ACPD
13, 8701–8767, 2013

upon the collision of an interstitial particle and a supercooled droplet and lastly immersion/condensation freezing, where a single particle fully/partially immersed in water will aid freezing of a supercooled droplet by stabilising (reducing the Gibb's Free Energy) the ice nucleation process at the surface of the immersed particle. By convention, condensation freezing is thought to take place when freezing follows water condensation on a particle at temperatures below 273 K (Murray et al., 2012 and references therein; Hoose and Möhler, 2012).

Heterogeneous ice nucleation on the surface of mineral dust (MD) particles has been studied extensively in previous laboratory and field studies (Hoose and Möhler, 2012; Murray et al., 2012 and references therein; Cantrell and Heymsfield, 2005). This class of particles is considered to be one of the most effective heterogeneous ice nuclei (IN) amongst biological particles (Pratt et al., 2009), bacteria, pollen and diatoms (Alpert et al., 2011; Knopf et al., 2011; Möhler et al., 2007). Airborne MD has the largest emission rate and average aerosol optical depth of all aerosol types (Satheesh and Moorthy, 2005). Due to the large burden of MD up to 1500 $\mathrm{Tg\,yr^{-1}}$ (Satheesh and Moorthy, 2005; Andreae and Rosenfeld, 2008), the potency of dust storms and the long residence time of several weeks in the absence of precipitation in the troposphere (Prospero, 1999), significant amounts of MD particles undergo long-range transport and get lofted to altitudes as high as 6 km within the Saharan Air Layer (Colarco et al., 2003). A number of field studies that observed the chemical composition using single particle mass spectrometry found MD particles that have undergone long range transport (typically from Asia or Africa to the USA) were enriched in ice crystal residuals. These particles were sampled through an IN counter that heterogeneously activated ambient particles from the upper free troposphere (DeMott et al., 2003a; Richardson et al., 2007) or as ice crystals directly in lee-wave-clouds (Field et al., 2012) and in convective cloud anvils (DeMott et al., 2003b; Cziczo et al., 2004). Field studies also report an enhanced ice crystal number concentration in clouds in the presence of dust storms (Sassen et al., 2003; Cziczo et al., 2004; DeMott et al., 2003b) suggesting the importance of dust to ice formation in the troposphere. Investigations of ice nucleation properties in the

ACPD
13, 8701–8767, 2013

deposition and condensation/immersion mode for a variety of MD such as Arizona Test Dust (ATD), Asian dust, Canary Island dust, kaolinite (Ka), illite, Israeli dust, montmorillonite and Saharan dust as a function of temperature (T), onset relative humidity (RH) and normalised to surface area of the aerosol particles have been elegantly reported (Hoose and Möhler, 2012 and references therein; Murray et al., 2012 and references therein). Laboratory based studies that focussed on ice nucleation of MD consistently show that there is a significant particle size dependency in all, deposition, immersion/condensation and contact modes (Kanji and Abbatt, 2010; Niemand et al., 2012; Lüönd et al., 2010; Welti et al., 2009, 2012; Ladino et al., 2011; Archuleta et al., 2005; Koehler et al., 2007) for defining ice nucleation onsets as a function of T and/or RH. These studies consistently conclude that larger particles are more effective heterogeneous IN requiring lower RH or less supercooling for the onset of ice formation. It is also evident that ice nucleation depends on surface composition of the particle (e.g. Kanji et al., 2008). Under the broad category of MD it is difficult to quantify the most effective atmospherically relevant MD IN. Recently a study by DeMott et al. (e.g. 2010) showed that for predicted concentrations of IN to agree with observed IN concentrations, parameterisations needed to be based on the number of particles that had diameters larger than 500 nm, suggesting that in the atmosphere there is a tendency towards larger particles acting as IN.

Ice nuclei parameterisations from previous laboratory studies that are used to extrapolate IN concentrations in the field, generally over predict IN concentrations (Eidhammer et al., 2009). Parameterisations of IN concentrations based on laboratory studies (Marcolli et al., 2007; Diehl and Wurzler, 2004; Lüönd et al., 2010) however, are based on experiments with "clean" MD and may not be representative of what is found in the atmosphere due to the long range transport atmospheric particles undergo. It is expected that aerosol particles in the atmosphere will interact with other atmospheric species such as trace gases and (in)organic aerosols. Ambient air containing Asian dust that was analysed for chemical composition using single particle mass spectrometry revealed that the MD can be internally mixed with sulphate and chloride (Sullivan

ACPD
13, 8701–8767, 2013

et al., 2007a,b) and organics such as oxalic and malonic acids (Sullivan and Prather, 2007). In a study where filter samples were collected during a dust storm in Beijing and analysed using transmission electron spectroscopy, dust was also found dust to be internally mixed with nitrate (Li and Shao, 2009).Laboratory ice nucleation experiments of MD coated with sulphates/sulphuric acid showed that for a given temperature, ice formation of sulphate coated particles was suppressed in the deposition mode requiring higher RH_i to activate (Archuleta et al., 2005; Cziczo et al., 2009; Eastwood et al., 2009) and depending on particle size, smaller coated particles ≤ 100 nm required homogeneous freezing conditions to nucleate ice (Archuleta et al., 2005). Similarly, for large MD cores immersed in ammonium sulphate solution drops, heterogeneous freezing was observed, however, for droplets with cores ≤ 100 nm, homogeneous freezing temperatures (~ 235 K) were required for ice formation (Hung et al., 2003). Deposition freezing was also found to be greatly suppressed when ATD particles were coated with sulphuric acid requiring water saturated conditions for ice formation and resulted in a lower fraction of particles being ice active compared to uncoated ATD (Sullivan et al., 2010b). Immersion freezing of 300 nm ATD particles showed a change in onset freezing temperature from 245 to 239 K when particles were coated with sulphuric acid (Niedermeier et al., 2011a,b). Ice nucleation of ATD particles exposed to nitric acid vapour (Sullivan et al., 2010a), showed impeded ice formation in the deposition mode and no effect of suppression in the condensation mode. In fact condensation freezing was found to be initiated at RHs just below water saturation (98 %) for particles exposed to nitric acid vapour suggesting sub-saturation condensation freezing. Kanji et al. (2008) found that octyl-coated silica particles impede ice nucleation in the deposition mode to beyond instrument detection limits compared to uncoated silica particles. Möhler et al. (2008) showed that coating illite particles with a surrogate of secondary organic aerosol (SOA) suppressed the ice nucleation ability in the deposition mode with the coated particles requiring 40 % higher RH_i than the uncoated particles. All of the above studies consistently observed that heterogeneous ice formation is suppressed due to processes that mimic atmospheric chemical ageing of MD particles.

ACPD
13, 8701–8767, 2013

However, field studies in Mexico City and Los Angeles in which atmospheric particles composed of organic coatings with soot or inorganic inclusions collected on ice nucleation substrates exhibited efficient immersion mode ice nucleation in the temperature range 233–230 K at RH_w as low as 90 % (Wang et al., 2012). From the same field study conducted in and around Mexico City, particles with dust and sulphate species coated with thin and thick layers of secondary organics did not show significantly different deposition mode ice formation onsets in the temperature range 240–205 K indicating that the level of ageing did not matter for ice formation onsets which were found to be in the range RH_w = 70–90 % (Knopf et al., 2010). Additionally, in a study conducted at a mountain-top site in Colorado (Storm Peak, 3210 m a.s.l.), ice crystal residual compositions were found to be enriched in minerals lending support to the efficiency of dust IN, however most ice active aerosol was found to contain detectable amount of organic material that had oxygen signatures (Baustian et al., 2012). The contrast between the laboratory and field studies suggests that the proxies of coatings used in the laboratory may not be fully representative of atmospheric compositions. It is possible however, that particle mixing state and ageing extent will differ based on their origin and trajectory as well as depending on where they are sampled.

The previously discussed field studies by DeMott et al. (2003a), Cziczo et al. (2004) and Richardson et al. (2007) found that the majority of MD particles in ice crystal residuals were not internally mixed with sulphates or organics. A study by Twohy and Poellot, (2005) where ice crystal residuals were sampled from anvil cirrus clouds onto filters and analysed by transmission electron microscopy also showed that the industrial and mineral dust categories were not mixed with sulphate and organics. It is therefore reasonable to conclude that laboratory studies of ice nucleation using bare mineral dust particles is of significant importance to understanding heterogeneous ice nucleation (Cziczo et al., 2004). The single mass spectrometric techniques used to investigate the mixing state of ice crystal residuals and aerosols are not sensitive to surface functional groups. Since MD is largely composed of oxides (mainly alumina and silica), one cannot eliminate the possibility of aerosol processing and oxidation reactions that

ACPD
13, 8701–8767, 2013

would lead to modification of the MD surface functional groups from exposure to trace gasses such as O_3 (Cwiertny et al., 2008).

Ozone is an important trace gas in the troposphere with an annual source of 3700–5400 Tg yr^{-1} and concentrations ranging from as low as 5 ppbv near the surface in clean regions up to about 120 ppbv in the upper troposphere in mid-latitudes. Global 3-D models have shown ozone concentration decreases by up to 10 % in dust source or nearby regions (Dentener et al., 1996). An airborne field study report reduced ozone mixing ratios within North African dust layers suggesting a loss of 4 ppbv O_3 day^{-1} (de Reus et al., 2000). A number of laboratory studies have shown that in the presence of MD or metal oxide surfaces, O_3 is lost to the particle surfaces (Roscoe and Abbatt, 2005; Chang et al., 2005; Sullivan et al., 2004; Usher et al., 2003b; Michel et al., 2003, 2002; Hanisch and Crowley, 2003; Li and Oyama, 1998; Li et al., 1998; Karagulian and Rossi, 2006; Mogili et al., 2006). In particular in the work of Roscoe and Abbatt, (2005) it was shown that the exposure of dry alumina to O_3 resulted in an irreversible stable IR absorption feature that was assigned to an M=O type functional group, where the M is a strong Lewis acid surface site with an anion vacancy on the alumina surface presenting evidence for a surface oxide species forming. A surface peroxide species formation was reported from Raman spectroscopy of manganese oxide exposed to O_3 presenting additional evidence of surface modification due to O_3 exposure (Li et al., 1998; Li and Oyama, 1998).

Given the tropospheric abundance of O_3, the long residence time and transport range of mineral aerosol, and the known interactions between O_3 and mineral particles, we present the ice nucleation properties of surrogates of atmospheric MD that have undergone exposure to O_3 at time scales ranging from short to long exposure in the atmosphere. To this date there is only one other study that has looked at the effect of O_3 exposure on MD particles. Specifically on montmorillonite, it was concluded that for an exposure at 200 ppbv, there was no evidence of change in the ice nucleation activity in the deposition mode (Salam et al., 2008). However the study only reports a single O_3 concentration, mode of ice nucleation and MD species. In this work we

ACPD
13, 8701–8767, 2013

address three specific questions; first, does the ice nucleation activity of the O_3 aged particles change and how? Second, is the effect uniform across different MD species and ice nucleation mechanisms? Third, is the effect dependent on the amount of ozone exposure? In order to answer these questions we compare the IN activity of untreated Ka and ATD in the deposition and immersion mode to that of O_3 aged Ka and ATD subjected to high and low O_3 exposures.

2 Experimental methods overview

A brief overview of a typical experiment is presented here and in following subsections we provide details of each part of the experiment. We used a single component mineral substance, kaolinite (Ka) and a desert dust representing a mixture of components, Arizona Test Dust (ATD). Polydisperse Ka particles (KGa-1b, Clay Mineral Society, $Al_4(OH)_8Si_4O_{10}$, density $= 2.2\,g\,cm^{-3}$) and ATD particles (fine dust, 0–3 µm nominal size, Powdered Technology Inc., density $= 2.65\,g\,cm^{-3}$) were suspended in a $2.78\,m^3$ cylindrical stainless steel aerosol tank with a diameter of 1.49 m in the middle of the tank and height of 1.91 m as shown in Fig. 1. The purchased ATD sample is milled, washed and baked at high temperature in its production process while the KGa – 1b particles after being collected from their field source deposits, undergo low temperature drying only. Inside the aerosol tank, particles can be exposed to various levels of O_3(described in Sect. 3.1). Immersion freezing measurements of untreated and O_3-aged particles were conducted for $232\,K > T > 264\,K$ with a combination of the IMCA – ZINC (IMmersion ChAmber – Zurich Ice Nucleation Chamber) shown in Fig. 2 that has been described in detail in Lüönd et al. (2010) and Welti et al. (2012). Deposition mode experiments of the same particles were conducted for $232 < T < 252\,K$ with the Portable Ice Nucleation Chamber (PINC) as shown in Fig. 3 which is described in detail in Chou et al. (2011). By measuring the aerosol size distributions in the stainless steel tank, ice crystal numbers in PINC and the droplet/ice crystal ratio in IMCA – ZINC,

ACPD
13, 8701–8767, 2013

we are able to report ice activated fractions as well as ice active surface site densities (IASSD) of the particles sampled.

2.1 Aerosol generation and processing

A stainless steel aerosol tank housed dry suspended Ka, BET (gas adsorption) surface area $11.8 \pm 0.8\,m^2\,g^{-1}$ (Murray et al., 2011) or ATD particles, BET surface area $5.7\,m^2\,g^{-1}$ (Wagner et al., 2008). The tank has 20 connecting ports made up of 16 KF40 and 4 CF200 flanges that can be used to couple various instruments for analysis and characterization of its suspended contents. One of the 16 ports is used for a direct connection to the IN counters, PINC and IMCA-ZINC while others are used for the aerosol monitoring instruments. The larger connection ports were not utilised for the current work. The aerosol tank also has a motor on the outside to operate a mixing fan inside the tank that can be run at varying speeds from 0–5000 rpm. A schematic of the aerosol tank is shown in Fig. 1. A variety of aerosol and ambient monitoring instruments were coupled to the tank such as the Aerodynamic Particle Sizer (TSI Inc., APS 3221), Condensation Particle Counter (TSI Inc., CPC 3772) and Scanning Mobility Particle Sizer (SMPS, TSI Inc., Electrostatic Classifier 3080, DMA 3081, CPC 3010 with an impactor 0.071 cm). In addition, a relative humidity sensor (Tetra Tec Instruments, MF-Q12), pressure transducer (MKS, Full Scale 1000 mb) and 4 type K thermocouple sensors that are mounted on a taut wire which is mounted in a vertical but diagonally oriented fashion inside the aerosol tank to monitor the temperature homogeneity. To produce O_3, the tank is connected to a variable efficiency (40–100 % conversion) corona discharge O_3 generator (Taoture International Enterprises Inc., Generator 1000 BT-12) that is fed by a 1 lpm high purity synthetic air supply (purity 5.6). An automatic O_3 transmitter (Aeroqual series 940–03, Full Scale 0.500 ppm) equipped with an internal pump sampled 100 sccm of air from the tank to obtain O_3 concentrations at a time resolution of 30 s. In order to conduct ice nucleation experiments of particles not exposed to O_3, the tank was "cleaned" by evacuating it to pressures of less than 1 mbar using a vacuum pump (Pfeiffer Vacuum, UNO 65) and refilled with ultra high

ACPD
13, 8701–8767, 2013

purity N_2 (purity 6.0) consecutively (3–4 times) so as to reduce background particle counts in the tank to below 1 cm^{-3}. To achieve this background, 3–4 successive evacuation and refill runs were required whereas to further reduce the concentration to about 10^{-2} cm^{-3} the tank was purged over a weekend (48 h) with a 0.6 lpm flow of N_2. Typically the weekend purge is only conducted if the aerosol species being sampled was being changed. Commercially available samples of Ka and ATD were dry suspended by adding particles into the tank to a concentration of approximately 3500 cm^{-3} with a rotating brush generator (Palas, RBG 1000) via a cascade of two cyclones that confined the size distribution to mostly below 1 µm. During the filling procedure the CPC measurements are initiated to monitor particle concentration and immediately after the SMPS and APS measurements are conducted to obtain size and concentration distribution data. Representative sample number and surface distributions of both Ka and ATD approximately fit lognormal distributions and are shown in Figs. 4 and 5, respectively. For Ka the size range (diameter) of the particles was 0.1–2.0 µm with a mode of 0.8 µm and for ATD, 0.05–2.0 µm with a mode of 0.4 µm.

To age the Ka and ATD particles before conducting IN measurements, the tank is cleaned as described above to reduce background concentrations before O_3 was introduced into the N_2 filled tank. Ozone was generated by allowing 1 lpm of synthetic air to flow through the ozone generator at a 40 % conversion efficiency setting for 20–30 s divided up into 5–10 s spurts over a few minutes to allow for sufficient mixing time in the tank and for the ozone transmitter to respond with the real time concentrations. Once an O_3 concentration of 460 ppbv was reached, O_3 addition was terminated and concentration in the tank was monitored for approximately 80–90 min in order to obtain the background O_3 decay (wall loss rate) as shown in Fig. 6. Aerosol particles are subsequently introduced into the tank until the desired concentration (typically $\sim$ 3500 cm^{-3}) is reached. The particles are allowed to age in the O_3 environment for approximately 2 h before IN sampling begins. All O_3 ageing experiments of the mineral dust particles were conducted under dry ($RH_w < 5$ %) and dark conditions at stable room temperature of 296 K with a variation of up to 0.2 K along the height of the aerosol tank. Using

ACPD
13, 8701–8767, 2013

the O_3 concentrations and aerosol mass concentrations obtained from the SMPS and APS, we determined the wall-loss of O_3 and uptake onto the dust particles. IN experiments where the dust particles were exposed to high concentrations of O_3 of 1.4 ppmv and 4 ppmv were also conducted. Uptake coefficients were only determined for the low concentration (460 ppbv) experiments since the uptake occurred fast and immediately after the addition of the dust to the O_3 filled tank and was on the order of 30–130 ppbv which is small compared to the large concentrations used for the high exposure experiments. In addition the instrument used to monitor real time O_3 concentrations had an upper limit of 500 ppbv. For the high exposure experiments, we injected a known amount of O_3 (calculated from air flow, time and conversion efficiency of the O_3 generator), and aged the particles for the same time as in the low exposure experiments. Based on the low concentration exposures and previously reported literature (see sections below) we assume that under these conditions O_3 is still lost to the particle surface but with different kinetic parameters and possibly different loss mechanisms. We note that determining O_3 uptake coefficients is not the focus of the current work, we present them in Sect. 4.1 to validate the O_3 uptake observed here and to compare our values to the large body of data that already exist in the literature which focussed on the kinetics and mechanisms of O_3 uptake onto MD (Usher et al., 2003a; Cwiertny et al., 2008 and references therein).

2.2 Ice nucleation measurements

Immersion and deposition mode IN counters sampled particles from the sampling port located at the top of the aerosol tank. The IN counters are of the continuous flow diffusion chamber (CFDC) design based on the original thermal gradient diffusion chamber principle (Rogers, 1988). The IN counters have been extensively described in previous work. An overview of their operation and detection is presented in the following sections while readers are referred to the relevant articles where details on the instruments' performance, characterisation and validation measurements can be found.

ACPD
13, 8701–8767, 2013

2.2.1 Deposition nucleation experiments with PINC

Deposition mode experiments were carried out with a CFDC that is compact and designed for field and portable applications. PINC (Fig. 3) is a parallel plate vertically oriented chamber with a distance of 10 mm between the two walls of the chamber and has been used and described extensively in previous work (Chou et al., 2011, 2013). Briefly, an aerosol layer is sandwiched between two particle-free sheath flows in the chamber whose inner walls are coated with ice and held at different temperatures. The total flow rate in the chamber is 10 L min^{-1} with the aerosol and particle-free sheath flows maintained at 1 L min^{-1} and 2 × 4.5 L min^{-1} respectively, on either side of the aerosol layer. The sheath flow constricts the sample to a known position between the two walls with reasonable accuracy in order to determine the sample temperature and RH. A typical experiment in PINC is conducted by setting both wall temperatures to the desired sample temperature followed by increasing the difference in temperature between the two walls resulting in a linear water vapour pressure field developing between the warmer and colder wall and the RH profile between the two chamber walls can be calculated. By knowing the position of the aerosol layer, it is possible to determine the RH the sample layer is exposed to. Particles that nucleate ice are detected by an optical particle counter (OPC, Climet 3100) that differentiates ice crystals from background particles based on particle size. The dust sample flow enters the main chamber (growth section) through a particle impactor with an aerodynamic diameter cut-off, d_{50} of 1 µm. This is necessary to cut out large particles that could be miscounted as ice by the OPC. The particles have a residence time of 7 s in the growth section after which the sample flow passes through an evaporation section (held at RH_{ice} = 100 %) for 2 s before exiting the chamber through the OPC. The evaporation section ensures that any water drops that may have nucleated will evaporate preventing anomalous ice counts by the OPC. In the current work, PINC was operated for deposition mode sampling in the range 253–232 K with a maximum corresponding sampling RH with respect to water (RH_w) of 104–112 %. The maximum RH is the point beyond which water droplets

ACPD
13, 8701–8767, 2013

grow large enough to survive the evaporation section in sizes not distinguishable from ice crystals and is referred to as the water droplet survival line as shown in Fig. 7. Aerosol sample concentrations decayed over the course of a sampling day due to settling and wall-losses in the tank, from ~3500 to 700 particles cm^{-3}. The number of particles is well below the maximum concentration of 7000–10 000 particles cm^{-3} that would cause any water vapour depletion in PINC. Particle coincidence errors in the CPC/OPC only occur at 10 000 particles cm^{-3} and are therefore not a concern in the current work.

2.2.2 Immersion freezing experiments with IMCA – ZINC

Immersion mode freezing experiments were conducted using a similar operation principle as described above, with a CFDC instrument that has been described in detail elsewhere (Lüönd et al., 2010; Welti et al., 2012). This instrument is divided into two parts, first the droplet activation of the dust particles and second the freezing section as shown in Fig. 2. The first part, IMCA consists of two vertically oriented parallel plates that are 5 mm apart in which dust particles are forced to act as condensation nuclei. The chamber walls are lined with continuously wetted filter paper and held at 323.2 K at the warm and 303.2 K at the cold wall in order to maintain RH_w = 110 % at 313.2 at the sample position. An aerosol flow of 1 L min^{-1} is sandwiched between particle-free sheath air of 2 × 2 L min^{-1} (total flow rate of 5 L min^{-1} in IMCA). The residence time in IMCA is 8 s. These conditions produce droplets of approximately 10 µm in diameter. After the droplet activation of the particles, the droplets are cooled in the lower part of IMCA just before being introduced into ZINC (Stetzer et al., 2008), the second part of the immersion freezing instrument. ZINC is also a vertically oriented parallel plate chamber whose internal walls are 10 mm apart, coated with ice and held at temperatures such that the aerosol layer is held at the desired temperature of observation for immersion freezing. Before the particles enter ZINC an additional sheath flow of 2 × 2.5 L min^{-1} is added, thus bringing the total flow rate in ZINC to 10 lpm with a residence time of just over 10 s in the supercooled region relevant for ice nucleation. The

ACPD
13, 8701–8767, 2013

RH_w in ZINC is maintained at 100 % so as to avoid the evaporation of or condensation onto the droplets.

In the current work, ZINC operates in an almost identical fashion to PINC. However, the ice detection methods between ZINC and PINC differ. For the IMCA – ZINC experiment ice detection is achieved with the Ice Optical DEtector (IODE) described in Nicolet et al. (2010). The IODE detector is mounted at the upper end of the ZINC evaporation section. IODE is a single particle instrument and therefore it is necessary not to have large particle concentrations in order to avoid coincidence errors in the depolarization ratios measured. In this work an average of 150–300 particles cm^{-3} was used in the immersion freezing experiments. Particles sampled by IMCA also passed through a 1 µm impactor to be consistent with particle sizes sampled by PINC. The detector used in IMCA is also sensitive to un-activated particles that are larger than 2 µm and potentially miscounts them as ice crystals.

IODE actively discriminates between ice crystals and liquid drops based on the principle that backward scattering on ice crystals will partly change the polarisation linear polarized incident light whereas spherical water droplets will not. IODE is an in-house self developed detector that has been tested and characterised as well as used for previous ice nucleation studies (Lüönd et al., 2010; Welti et al., 2012; Ladino et al., 2011; Nicolet et al., 2010). The single plane parallel polarized laser light is aligned to the sample layer passing through ZINC and particles are classified to be ice crystals or water droplets due to the intensity of parallel and perpendicular polarized components of backscattered laser light. The signal collected is corrected for background signal from aerosol-free flow from the IODE detector that can come from reflections within the ice chamber and internal reflections within IODE. More details about the detection and signal collection with IODE can be found in Lüönd et al. (2010). Uncertainties are addressed in the following section.

ACPD
13, 8701–8767, 2013

2.3 Instrument and measurement uncertainties

The uncertainties in all the measurements reported have been determined through error propagation based on individual instrument uncertainties. All data points shown are an average of 2–4 repeated experiments, therefore we have plotted instrument uncertainties as the error bars. For all derived parameterizations we have included the error bar weighing when determining the fits. The relative uncertainties in particle concentrations reported from the CPC and OPC are both 10 %. The uncertainty in RH reported for PINC and ZINC for the temperature range relevant to this work is ± 2 % (Chou et al., 2011) which mostly comes from the uncertainty in temperature measurement of ± 0.1 K and the corresponding equilibrium vapour pressures of ice and water. This uncertainty results in a temperature variation across the aerosol lamina of ± 0.4 K. The uncertainty in ice active fractions (AF) for the deposition mode data is ± 14 % (error bars plotted but not immediately visible in Fig. 8). For the immersion freezing data, the frozen fractions are based on individual particle counts and each frozen fraction is the result of classifying between 2000–3000 particles into the ice or droplet categories. The classification of ice or water is based on a threshold depolarization in IODE. If this threshold is met, then a particle is classified as ice. However if the depolarisation signal of the particle is within 1σ standard deviation of this threshold, then the particle counted is potentially misclassified. The uncertainty in frozen fraction which we also refer to as activated fraction, AF (see error bars in Fig. 9) is therefore the ratio of potentially misclassified droplets (+ error) or ice crystals (– error) to the total number of detected particles. As such for each frozen fraction detected, the uncertainty varies. For additional details on the signal analysis we refer readers to Lüönd et al. (2010). The uncertainties in IASSD are propagated from the uncertainties in the optical detection methods (OPC and IODE) and the aerosol counting instruments (CPC/SMPS) and shown as error bars in Figs. 10 and 11. Lastly, the measurement uncertainty from the O_3 transmitter in the concentration range 0.001–0.5 ppm is reported to be ± 2–5 %.

ACPD
13, 8701–8767, 2013

3 Results

We present the results in three subsections. First we discuss the O_3 uptake kinetics observed during ageing experiments (absolute amount of O_3 taken up, surface coverage by O_3 on the dust particles and uptake coefficients) and compare our results to the literature to show consistency of the results obtained here. In the second and third part we present the data on the ice nucleation of untreated and aged Ka and ATD particles in the deposition and immersion mode.

3.1 Ozone ageing experiments

Time series of O_3 decay from two experiments, one with Ka and the other with ATD in the absence of particles (wall-loss) and presence of particles is shown in Fig. 6. It is evident from these plots that there is a larger loss of O_3 in the presence of the MD which can be attributed to both reactive uptake and catalytic destruction (Sullivan et al., 2004). From the data obtained here (red points in Fig. 6) we deduced rate constants of O_3 decay by assuming first order O_3 loss to the MD particles (Chang et al., 2005; Sullivan et al., 2004; Karagulian and Rossi, 2006; Usher et al., 2003a,b; Michel et al., 2002, 2003; Hanisch and Crowley, 2003). The absolute uptake of O_3 was derived (see Eq. 1) by taking the difference in concentrations between the background period (black points) and the ageing period where the O_3 loss rate had returned to that in the absence of particles (green data points in Fig. 6). This was done by linearly extrapolating the black and green data points and taking the average difference in O_3 concentration between the lines at three different times along the time series. This was repeated for 2 additional ageing experiments for each Ka and ATD. From the amount of O_3 lost to the MD particles and the BET surface area of Ka and ATD, we determined the active surface site coverage of Ka and ATD using the following equation:

$$\text{surface coverage} = \frac{[O_3]_{\text{uptake}}(\text{molecules cm}^{-3})}{SA_{\text{aerosol}}(\text{cm}^2\,\text{cm}^{-3})} \quad (1)$$

ACPD
13, 8701–8767, 2013

The surface coverage serves to indicate the amount of O_3 that is destroyed per unit surface area of dust particulates, i.e. the number of sites capable of interacting with O_3. The O_3 loss per unit surface area is higher for ATD than is for Ka, contrary to what one would expect from observing the data in Fig. 6 which shows the net uptake was lower on the ATD samples. However this is not surprising given that the BET surface area of Ka is a factor of two more than ATD. Additionally the surface coverage also serves to indicate if the loss is catalytic on the MD surface. The values in this work are on the order of 10^{15} and 10^{16} molecules cm^{-2} for Ka and ATD respectively, whereas the number typical for the maximum number of sites available on a hexagonally closed pack crystal such as Ka and metal oxides (silica and alumina) which form 85 % of the ATD composition is roughly 10^{15} sites cm^{-2}. Assuming one molecule bound per surface site, the surface coverage reported here suggest that the ATD surface does not saturate immediately but potentially displays catalytic behaviour to some extent whereas the Ka surface appears to be less catalytic in its O_3 uptake (Michel et al., 2002; Sullivan et al., 2004).

Using the method described in Cwiertny et al. (2008) and the rate constant from the initial first order loss of O_3 on the dust (k_{obs}), we determined initial uptake coefficients using the following relationship:

$$k_{obs} = \frac{\gamma c_{O_3} S_{BET} C_{mass}}{4} \quad (2)$$

where γ is the initial uptake coefficient, c_{O_3} is the mean speed of O_3 (392 m s^{-1}), C_{mass} (g m^{-3}) is the mass concentration of the aerosol species taken from the peak concentration aerosol distributions using the densities given in Sect. 3 and S_{BET} is the BET surface area (m^2 g^{-1}) given in Sect. 3.1. Results are listed in Table 1.

The uptake coefficients determined from our work are comparable to those obtained in previous kinetic studies of O_3 uptake on MD particles also based on BET surface areas. For example, an uptake coefficient reported by Michel et al. (2003) for Ka was $(3 \pm 1) \times 10^{-5}$ which is comparable to the values we obtain for Ka listed in Table 1.

ACPD
13, 8701–8767, 2013

Hanisch and Crowley (2003) report an uptake coefficient of 1.2×10^{-4} for Saharan dust which also compares well to the values listed in Table 1 for ATD. Despite the different source of dusts here, we note that ATD shares a major component, quartz (SiO_2) with Saharan dust. Arizona Test Dust also contains iron (iii) oxide which has been reported to have an uptake coefficient of $(1.8 \pm 0.7) \times 10^{-4}$ (Usher et al., 2003a) and is also comparable to our values for ATD. Furthermore, an uptake coefficient for ATD of $(2.5 \pm 1.2) \times 10^{-3}$ has been reported for an initial O_3 concentration of 8×10^{12} molecules cm^{-3} (Karagulian and Rossi, 2006). Given that our initial concentrations are on the order of 1×10^{13} molecules cm^{-3} (430 ppbv) and we have an order of magnitude lower uptake coefficients for ATD (on the order of 10^{-4}), our uptake coefficients are in good agreement in light of previous observations that report uptake coefficients to inversely correlate with initial O_3 concentrations since the ratio of O_3 molecules taken up by the dust surface to the number of O_3 molecules colliding with the surface decreases (Sullivan et al., 2004; Hanisch and Crowley, 2003).

The dry conditions used in this study are atmospherically relevant as it has been shown previously that water vapour does not affect the kinetics and initial uptake coefficient of O_3 on MD for both alumina (Sullivan et al., 2004) and authentic Saharan dust (Chang et al., 2005) lending support to the interaction of MD with O_3 in the atmosphere. Additionally, such interactions on freshly emitted dust are expected to occur in drier parts of the troposphere inside dust plumes or the Saharan Air Layer.

Typical background O_3 concentrations in the troposphere are on the order of 30–60 ppbv between 2–11 km altitudes and in urban regions with high NO_x sources present, the concentrations can range from 100–400 ppbv causing serious pollution challenges (Usher et al., 2003a and references therein). For example, during global dust transport in a Saharan Air Layer, it is very common to encounter the altitudes between 2–4 km (Zipser et al., 2009) so that dust particles are exposed to typical O_3 concentrations consistently for several days such that ozone depletion onto Saharan dust has directly been observed (de Reus et al., 2000). Prior to being lofted into the

ACPD
13, 8701–8767, 2013

upper troposphere, dust can be transported through heavily polluted regions, e.g. Beijing, where it can get exposed to [O_3] as high as 120 ppbv (Streets et al., 2007).

We extrapolate the exposure time and O_3 concentrations in our work to the atmosphere by estimating a chemical ageing time. For our low exposure particles aged at initial [O_3] of 430 ppbv and an exposure time of 130 min we get a chemical age of 55 900 ppbv minutes. Assuming an atmospheric background concentration of 45 ppbv in the mid-upper troposphere, the mineral dust particles would need to have a residence time of ~ 1 day in order to achieve a similar level of ageing as the low exposure experiments presented here. Our chemical age of 1day is atmospherically relevant given the long residence times of MD in the atmosphere of up to 1–2 weeks. Similarly for the high [O_3] experiments we also expose the MD particles for ~ 130 min for an initial [O_3] of 1.4 ppmv and 4.3 ppmv. If we assume 45 ppbv atmospheric background concentrations, this would correspond to ~ 3 and 9 days of atmospheric ageing, respectively. To reflect dust transport through a polluted region, we use an [O_3] of 100 ppbv, the chemical ages calculated above are reduced to 9 h, 30 h and 4 days for 130 min of ageing at 0.43, 1.4 and 4.3 ppmv of O_3, respectively. A chemical age of 9 days approaches the limit of the residence time of MD particles in the troposphere in which time other species such as organics and sulphates are likely to be involved in the ageing process. A chemical age of 1 and 3 days is a reasonable time for MD to be exposed to typical background O_3 concentrations. On the other hand during a dust storm, particles can be transported through a polluted urban region where the O_3 concentration is 100 ppbv and thus 9–30 h could be representative of such events.

Lastly, we note here that the [O_3] used in our low exposure studies are a factor of 4–10 higher than encountered in the troposphere. Uptake of O_3 onto MD is known to occur via the Langmuir type mechanism (Usher et al., 2003a) which implies at lower [O_3], uptake could proceed faster and surface coverage may not approach surface saturation as in the current work. For convenience from here on we refer to the untreated particles by their names, Ka and ATD whereas the low exposure particles will

ACPD
13, 8701–8767, 2013

be prefixed with LE and the high exposure with HE to represent shorter and longer ageing times, respectively.

3.2 Deposition mode ice nucleation

In Fig. 7 the onset RH_w for 0.1 % AF of Ka and ATD as a function of temperature for the untreated, LE and HE particles are shown. Studies of hygroscopicity have shown that ATD is non-hygroscopic at sub-saturated water conditions (Koehler et al., 2009) for particles with diameters larger than 100 nm (Vlasenko et al., 2005) which applies to the majority of the ATD particles in this work. Hydrophobic properties of Ka have also been reported through atomic force microscopy measurements (Yin and Miller, 2012). Therefore it is unlikely that Ka takes up water at $RH_w < 100$. Data in the region above water saturation are therefore interpreted as ice formation via condensation freezing and for those below water saturation we infer deposition nucleation. The Ka particles (Fig. 7a) show no deposition mode activity at $T > 240$ K for 0.1 % AF, however at $T < 240$ K, deposition mode nucleation is active and the onset RH_w required to activate 0.1 % reduces with temperature. For $T > 240$ K we cannot report condensation freezing unambiguously on Ka particles because AF of 0.1 % is detected in the region beyond our ice crystal detection, i.e. in the water drop survival region where the OPC cannot discriminate between ice and water. The Ka sample used appears to be a relatively weak IN compared to ATD in the deposition mode. Deposition mode studies on Ka reported for the same temperature range studied in this work but for onset RH_w defined at ~0.5–1 % AF found consistently lower RH_w by 5–8 % for $233 < T < 253$ K (Salam et al., 2006). There are however three important differences to note here, first, the mode particle size used in the Salam et al. (2006) study of 1.5 µm is significantly larger than the particle size mode used here of 800 nm, thus the higher onset RH_w in our work is expected. Second, the residence time in the Salam et al. (2006) work is 20–30 s, which is on the order of 3–4 times more than for PINC which could result in a higher ice fraction being nucleated. Third, the Ka source from the Salam et al. (2006) study is not the same as that used here. Deposition mode data at the 1 % AF level are

ACPD
13, 8701–8767, 2013

reported in Welti et al. (2009) for Ka (Fluka) for 100, 200, 400 and 800 nm. Despite the latter size being similar to the mode size of our polydisperse sample, the onset RH_w are approximately 15 % lower than what we report here for 0.1 % AF at for example, 238 K indicating the their sample was much more active than the one used in this work. Recent studies have reported that the Ka particles from Clay Mineral Society as used in the current work exhibit lower IN activity compared to other commercially available samples (Pinti et al., 2012; Murray et al., 2012) albeit in the immersion mode. Deposition mode studies using the same Ka as this study have also been reported, however using an environmental scanning electron microscope (ESEM) with larger particle sizes of 1–10 µm (Zimmermann et al., 2007). ESEM is sensitive to the first ice nucleation event out of a particle population and performed with particles on a substrate (cold stage). The combination of the method and the size of the particles make it difficult to compare the results and not surprisingly the results from Zimmermann et al. (2007) showed that for Ka particles, deposition nucleation was active at T as warm as 253 K which is 13 K higher than what we observe.

The data for LE-Ka particles (green data in Fig. 7a), despite having onset RH_w that is within the detection uncertainty (except at ∼235 K), appear consistently at lower RH_w required to activate 0.1 % of the particles. This suggests that there may be a subtle enhancement of the ice nucleation of these particles when exposed to ∼430 ppbv of O_3, with the exception of the data point at ∼238 K which appears to have the same activity as Ka. The HE-Ka particles show a clear suppression of ice nucleation activity requiring higher RH_w to activate 0.1 % of the particles, indicating that longer O_3 ageing inhibits ice nucleation activity in the deposition mode. Given this suppression trend and the relatively weak ice nucleation activity of Ka at $T > 240$ K, we did not further explore the ice nucleation activity of the HE-Ka particles at $T > 240$ K as we were limited by instrument detection limits into the water droplet survival region.

The data for 0.1 % AF of ATD particles (Fig. 7b) indicate that deposition mode ice nucleation is active for $T < 250$ K above which we observe ice formation in the water saturated region. Similar deposition mode dependence on T has been inferred for ATD

ACPD
13, 8701–8767, 2013

in other studies conducted by different IN counters and an expansion chamber where the transition from condensation to deposition modes is reported to occur at ~250 K (Kanji et al., 2011). A study that used ZINC also found ATD to become active in the deposition mode between 250 and 246 K (Welti et al., 2009). These results suggest that ATD is an efficient IN activating in the deposition mode at T as warm as 250 K. Despite this efficiency, in our work at the colder T ~ 233 K, the onset RH_w for ATD is 3 % higher than for Ka supporting a higher efficiency of Ka over ATD. This may be surprising given the overwhelming evidence in the literature regarding ATD as being one of the most effective MD samples for ice nucleation (Hoose and Möhler, 2012 and references therein). However, if one looks at the size distributions of both the samples it becomes evident that due to the larger size mode of 800 nm for Ka compared to only 400 nm of ATD, that particle size is likely the cause for this earlier onset in ice nucleation on Ka particles (Archuleta et al., 2005; Welti et al., 2009; Kanji and Abbatt, 2010). For ATD at 0.1 % AF there is no significant difference between the aged ATD and ATD particles at a given temperature since the onset RH_w of ice formation fall within the instrument uncertainty limits. Despite this, we note that for the HE-ATD particles, in the deposition regime (T < 250 K), there is a consistent trend of a higher RH_w required to activate 0.1 % of the particles compared to the untreated particles, indicating there may be a small effect of ageing. Figure 7 does not represent the complete ice activation spectra observed since only a cross section of the ice activation spectrum at AF = 0.1 % is reported. We therefore present plots where we fix RH_w = 95 % and plot the AF as a function of T in Fig. 8. By choosing RH_w = 95 % we ensure that for all T plotted, we remain in the deposition regime, preventing any biases of increased AF from an onset of condensation freezing above water saturation.

With the data plotted as shown in Fig. 8a it is evident from the AF and corresponding exponential fits that there is a difference in deposition mode activity of the LE-Ka and Ka particles with the former being more efficient IN with higher AF at a given temperature. The data plotted here confirm with confidence the subtle inferred trend observed in Fig. 7a. Additionally, the HE-Ka shows a significantly lower AF than the

ACPD
13, 8701–8767, 2013

Ka and LE-Ka, thus confirming our conclusions drawn from data in Fig. 7a. The measurements suggest that long exposure to O_3 can be detrimental to IN activity for the temperature regime studied and the Ka sample used. This is reasonable considering atmospheric ageing of MD particles will tend to change properties of the surface thus changing their IN activity. However, it is surprising that ice nucleation of the LE-Ka and HE-Ka do not respond linearly, i.e. both suppressed or both enhanced, just by different magnitudes.

In Fig. 8b data are plotted for ATD with fits reported in Table 3, describing each of the particle populations. The LE-ATD and HE-ATD particles both show a reduced activated fraction and hence a suppression to ice nucleation in the deposition mode compared to ATD. In addition, the 95 % confidence interval bands (not shown here) for the fits of LE-ATD and HE-ATD, show that there is an overlap between the two data sets. For the LE-ATD with the exception of the point at $T \sim 243$ K, all other AF reported are consistently lower than ATD and the same applies for HE-ATD except for the point at 241.5 K. The representation of data in Fig. 8 and the observations made thereof are an indication that the cross section of data at AF = 0.1 % (as presented in Fig. 7) can be limiting and not fully representative of the ice activation spectra obtained for deposition mode nucleation, especially given the onset RH_w for both LE-ATD and ATD data were mostly within the instrument uncertainty in Fig. 7.

3.3 Immersion mode ice nucleation

In Fig. 9 we present the activated ice fraction (AF) from immersion freezing experiments as a function of temperature. The data indicate that the LE-Ka particles are also more effective IN in the immersion mode compared to the Ka particles. There is also a strong reduction of the ice nucleation ability of HE-Ka. Specifically, when one considers the median T at which half of the immersed particles catalyse freezing, ($T_{50\,\%}$), we observe a shift to warmer temperatures for the LE-Ka and a shift to colder temperatures for the HE-Ka as can be seen in Fig. 9a and reported in Table 2. In addition the onset temperature for immersion freezing, i.e. the highest temperature at which we

ACPD
13, 8701–8767, 2013

can detect ice formation is warmest for LE-Ka consistent with their enhanced efficiency compared to Ka. Also, the HE-Ka only shows an onset of freezing at temperatures colder than for Ka (see Table 2). However, we note that the AF corresponding to the onset freezing temperature is within the limit of detection (AF < 0.1) of IODE and thus should be treated with caution. Note that in Fig. 9a, the data points have been binned into 0.6 K temperature bins, i.e. data point ± 0.3 K of a nominal T to increase clarity and reduce clutter of the data points in the graph. Immersion freezing of identical Ka particles as used in this study also reported $T_{50\%}$ of 238 K for suspensions with 0.05 and 0.1 % by weight Ka (Murray et al., 2011) which corroborate our observations. Results from immersion mode studies of different Ka samples (Fluka), show a $T_{50\%}$ of 241 K for 800 nm particles (Lüönd et al., 2010), which is the mode diameter of the Ka particles used in this study. We note that the warmer $T_{50\%}$ is not surprising as the Ka from Fluka has been reported to be more active in the immersion freezing mode than the Ka used here (Pinti et al., 2012).

In Fig. 9b we show the immersion freezing results for ATD particles. These results somewhat corroborate the observations of the Ka particles. The similarity between Ka and ATD is the suppression of AF in response to the high O_3 exposure, as can be seen from Fig. 9 and the $T_{50\%}$ in Table 2. However, we note that for HE-Ka the suppression was also observed at T_{onset} whereas for ATD we find similar T_{onset} for HE/LE-ATD and ATD as shown in Table 2 indicating that the O_3 exposed ATD did not respond to T_{onset} in the same manner as the exposed Ka particles. However, at the relatively warm T_{onset} of ATD, the AF are $\ll 0.1$, which is below the detection limit of IODE. Evidence of non-uniform response between Ka and ATD comes from the absence of any significant difference between the AF(T) curves of ATD and the LE-ATD particles. Fits in Fig. 9b are weighed with corresponding error bars. If plotted with the 95 % confidence interval bands (not shown here), the datasets exhibit overlap over the measured temperature range. The immersion freezing of 300 nm ATD particles has been reported by Niedermeier at al. (2010), however $T_{50\%}$ occurred at $T < 236$ K in the homogeneous freezing regime, suggesting that the particles did not freeze heterogeneously in contrast to the

ACPD
13, 8701–8767, 2013

current work. However, we note that for our polydisperse sample, a particle mode of 400 nm implies a significant number of 600 and 700 nm particles. Although polydisperse measurements of ATD in the immersion mode have been previously studied (Connolly et al., 2009), $T_{50\,\%}$ were not reported.

The shaded region in Fig. 9 is the region where homogeneous freezing of 10 µm water drops is active derived from the work of Earle et al. (2010), thus we cannot attribute any freezing observed in this region to heterogeneous nucleation. We find that for the HE particles, this homogeneous freezing threshold is reached at lower AF of 65 % and 90 % for HE-Ka and HE-ATD, respectively. However for the LE and untreated particles, an AF of 100 % is reached before the homogeneous freezing threshold within experimental uncertainty. This behaviour indicates that the ageing has significantly inhibited immersion freezing of the HE-Ka and that approximately 1/3rd of the particles were unable to act as heterogeneous IN.

This is one of the first studies to show an inhibition of ice nucleation explicitly in the immersion regime due to ageing of dust particles at atmospherically relevant conditions. A study by Sullivan et al. (2010b) reports enhanced loss of IN activity of sulphuric acid coated ATD particles in the condensation – immersion regime, however the particles were heated during the coating process to $45\,^{\circ}\mathrm{C} < T < 85\,^{\circ}\mathrm{C}$ and the authors report that the effect of heating-coating combination could not be separated from that of coating (ageing) alone.

ACPD
13, 8701–8767, 2013

4 Discussion

4.1 Comparison of IN ability between deposition and immersion mode ice nucleation

4.1.1 Kaolinite

In the reported temperature range Ka responds uniformly to the ageing process with the LE-Ka yielding better IN than Ka and HE-Ka exhibiting a significant suppression in AF compared to Ka for both the immersion and deposition modes as shown in Figs. 8a and 9a. It is not entirely surprising that the trend observed the deposition nucleation is also mirrored in the immersion freezing mode because for both modes the particle surface catalyses the stabilisation of an ice germ on the particle surface. However, it is also possible that for a given mode, deposition or immersion, one of the two features, chemical or physical properties, play a more important role in determining ice nucleation. To specifically compare across different IN modes, we choose a convenient T of $\sim$ 235 K in Fig. 8a (deposition mode) and find that there is almost an order of magnitude difference in AF between the LE-Ka, Ka and HE-Ka in that order with LE-Ka being the highest. Comparing $T_{50\%}$ for the HE-Ka ($\sim$ 236 K) from Fig. 9a (immersion mode) to Ka and LE-Ka, yields the same activated fraction at 2 K and 4 K higher temperatures, respectively.

4.1.2 Arizona Test Dust

The AF of HE-ATD showed lower IN activity in both immersion and deposition modes. However the suppression observed for HE-ATD occurs to a lesser extent than in HE-Ka considering the following explanation. The O_3 concentration for HE-ATD (4.3 ppmv) is a factor of 3 more than HE-Ka (1.4 ppmv), but the AF in deposition mode is suppressed by a factor of 3–4 relative to ATD which is less than the extent of the suppression by a factor of 10 observed between HE-Ka and Ka (see Fig. 8a). Assuming

ACPD
13, 8701–8767, 2013

a linear relationship between deposition mode AF O_3 concentrations used for ageing, ATD would require an O_3 exposure of 10 ppm to produce the same suppression in the AF as that observed with HE-Ka. The same comparison can be made for immersion mode freezing. For HE-Ka to show the same suppression as HE-ATD an O_3 ageing concentration of $\sim$2.1 ppmv would be required as opposed to the 1.4 ppmv used for HE-Ka in our experiments. This simple comparison of ice nucleation efficiencies serves to show that the two species of MD particles responded differently to the O_3 ageing/uptake process as indicated by their uptake coefficients and their ice nucleation efficiency.

LE-ATD does not respond in the same manner as LE-Ka to ice nucleation is not surprising since MD with varying compositions are expected to show differing IN properties (e.g. Kanji et al., 2008; Archuleta et al., 2005). However, what is *initially surprising* is that from Fig. 8b it appears that LE-ATD and HE-ATD both show suppressed ice nucleation compared to ATD implying no effect of O_3 ageing concentration on ATD ice nucleation efficiency. However, if we quantify ice nucleation by normalising to the surface area of particles rather than to the number, we can obtain further clarity into this behaviour.

4.2 Parameterization of results using Ice Active Surface Site Densities (IASSD) as a function of temperature, $n_s(T)$(singular/deterministic approach)

This approach assumes that surface sites with specific activation energies that are equally distributed over the dust are responsible for ice formation in a wide range of freezing probabilities as a function of temperature and time. Studies have shown the dependence of ice nucleation on particle surface area in both immersion (Murray et al., 2012 and references therein) and deposition (e.g. Kanji and Abbatt, 2010; Wheeler and Bertram, 2012). In this parameterization time dependence is not taken into account similar to the work of Connolly et al. (2009) and Niemand et al. (2012) thus effectively following the singular or deterministic approach. In addition to the mentioned studies, justification for using the $n_s(T)$ parameterization comes from a number of reasons. In

ACPD
13, 8701–8767, 2013

a time dependence study of immersion freezing of Ka (Fluka) particles using the same instrument (Welti et al., 2012), we observed that the frozen fraction depended on time in the first 10 s, but for 11–22 s the frozen fraction did not change with time. Using the best-fit time dependent parameters and a lognormal aerosol distribution, model runs were used to extend the time dependent fits to 30 min to represent glaciation in a cloud. It was found that an order of magnitude increase in time would be required to produce the same frozen fraction resulting from a cooling of 1 K. i.e. a small change in supercooling will cause a much larger change in frozen fraction than will time, concluding that temperature is a much stronger predictor of frozen fraction compared to time (Welti et al., 2012). For deposition mode, the work of Wheeler and Bertram (2012) showed that the deterministic approach produced the best fit to their ice active fraction dependency on onset RH, contrary to what one would expect from classical nucleation theory. Lastly, in the work of Kanji and Abbatt (2006), a simple test was conducted where maintaining the RH_{ice} roughly 2 % below the onset RH_{ice} (determined apriori) for Saharan dust particles at approximately 233 K for 20 min or longer did not result in ice nucleation, however increasing the RH_{ice} to onset conditions resulted in ice formation within less than 0.4 s. IASSD serves as a convenient way to compare IN studies of monodisperse particles to those conducted with polydisperse particles, to implement laboratory results into climate models and to extrapolate to atmospheric ice crystal concentrations as is discussed in Sect. 6.

To parameterize our results, we determine $n_s(T)$, at a fixed RH for both ice nucleation modes. This can be done if we assume that the particles within a sample are of uniform composition and that $n_s(T)$ does not change with particle size. In the following, $n_s(T)$ is calculated as described in Hoose and Möhler (2012) for both immersion and deposition mode that are shown in Figs. 8 and 9.

$$n_s(T) = \frac{-1}{SA} \ln(1 - AF) \quad (3)$$

$$n_s(T) \approx \frac{AF}{SA} = \frac{N_{IN}}{SA_{tot}} \quad (4)$$

ACPD
13, 8701–8767, 2013

where SA (m^2) is the geometric surface area of a particle, AF is the activated ice fraction, N_{IN} is the ice crystal concentration ($\#\,cm^{-3}$) and SA_{tot} ($m^{-2}\,cm^{-3}$) is the surface area concentration of the polydisperse. The approximation (Eq. 4) is only valid for AF < 0.1 and therefore we use the approximation to only determine $n_s(T)$ for the deposition mode data which satisfies this criterion. Since the immersion mode data span AF > 0.1, we use Eq. (3) with the particle mode size of each sample to determine the SA, assuming spherical particles. The mode size of the dust samples does not change over the course of sampling from the aerosol tank, thus it is a reasonable assumption. In Figs. 10 and 11 we present the $n_s(T)$ for deposition mode and immersion mode ice nucleation, respectively.

The results for Ka in Fig. 10a for deposition mode mirror confirm those presented in Fig. 8a. The n_s of LE-Ka are 1 and 2 orders of magnitude higher than Ka and HE-Ka, respectively. The difference in n_s across the T range studied between the HE-Ka and LE-Ka implies that the corresponding residence times of 1–3 days (see end of Sect. 4.1) of dust the atmosphere could have an impact on their deposition mode ice nucleation properties. IASSD for Ka particles in the immersion mode are presented in Fig. 11a. We observe that n_s of LE-Ka is a factor of 5 more than Ka at warmer $T \sim 250$ K. At colder T, the n_s merge as the homogeneous freezing limit is approached with the difference being less than a factor of 2 at 233 K. Based on the fits, the n_s of HE-Ka does not differ significantly from that of Ka at warmer temperature, however on approaching homogeneous freezing temperature, there is a small difference of a factor of 2. The n_s for HE-Ka is smaller by a factor of ~2–4 with decreasing temperature compared to LE-Ka implying that the aerosol ageing concentration had a smaller impact in the immersion mode compared to deposition mode where the HE-Ka are ~100 times less active than the LE-Ka.

IASSD for ATD particles in the deposition mode are presented in Fig. 11b. When we account for n_s, we find that the ice nucleation activity of LE-ATD is not different from the ATD as was observed in the AF plots (Fig. 8b) where HE and LE aged particles responded with suppressed AF compared to ATD. This is a good illustration of

ACPD
13, 8701–8767, 2013

the importance of quantifying the ice nucleation activity of particles using surface area. Data in Fig. 10b suggest that there is no difference in ice nucleation behaviour between ATD and LE-ATD but there is a clearer suppression in nucleation efficiency of HE-ATD compared to the low exposure and untreated particles. IASSD for ATD in the immersion mode are presented in Fig. 11b. These corroborate the observations from the AF in Fig. 9b. If n_s fits of LE-ATD and ATD are plotted with 95 % confidence interval bands, overlap over entire T range is found (not shown here). There is approximately an order of magnitude difference in n_s between HE-ATD and ATD at warmer $T \sim 256$ K. All n_s curves merge at colder temperature suggesting that surface changes due to O_3 ageing is playing a role at warmer temperatures, but as the homogenous freezing limit is approached, ageing matters less and temperature is the primary determinant for immersion freezing. This is not surprising, since it is expected that at $\sim 234 \pm 0.4$ K (where the data merge) the freezing is not catalysed by the surface of the particle and can occur in the volume of the droplet. The merging of the n_s fits at homogenous freezing temperature is also observed for the LE-Ka and Ka particles, however not for the HE-Ka (see Fig. 11a). As discussed in Sect. 4.3, this indicates that a subset of the HE-Ka were completely de-activated and unable to catalyse ice formation even at the coldest heterogeneous freezing temperature. The same behaviour was not observed with HE-ATD despite the higher O_3 concentration of 4.3 ppmv used compared to only 1.4 ppmv for HE-Ka supporting our discussion (Sect. 5.1.2) that higher O_3 concentrations would be required for ATD to show the same suppression as Ka. The relatively unperturbed production process of Ka compared to ATD (see Sect. 3) could mean that Ka have more environmental impurities associated with it than ATD. Confidence in the suppression of HE-Ka being due to the O_3 ageing comes from the fact that Ka and LE-Ka display 100 % activation (within experimental uncertainty) at $T \sim 234$ K as shown in Fig. 9a.

Lastly, the n_s for Ka and ATD in deposition mode at for example, $T = 235$ K, are ~ 2.5 orders of magnitude lower than that observed for immersion freezing, implying that the MD particles used in the current work have a surface that is more active in immersion

ACPD
13, 8701–8767, 2013

mode ice nucleation. In other words only a small fraction of particles out of a sample population are active to ice nucleation in the deposition mode for $RH_w = 95\,\%$, as is often indicated by the lower AF detected in deposition mode studies.

4.3 Effect of O_3 ageing on the ice nucleation of Ka and ATD particles

In this section we suggest reasons for the change in ice nucleation behaviour observed in the particles due to O_3 ageing. In particular, we discuss the non-linear change in ice nucleation ability observed for the LE and HE O_3.

4.3.1 Effect of low O_3 exposure

Enhancement of the IN ability of the Ka particles exposed to O_3 is reasonable given that O_3 is a powerful oxidant and is known to react with mineral and oxide surfaces making them more hydrophilic. Increased water vapour adsorption on alumina surfaces pre-treated with O_3 has been observed in association with the surface species appearing in the form M=O (Roscoe and Abbatt, 2005). Mechanisms whereby an O atom becomes incorporated into MD surfaces upon O_3 exposure has been proposed in a number of studies (Usher et al., 2003a and references therein). Such surface oxide species can play a role in stabilising a water cluster through dipole intermolecular forces with the H_2O molecule thus lowering the energy barrier of ice germ formation (Pruppacher and Klett, 1997). Increased water vapour uptake observed at $RH_w = 90\,\%$ onto ozone treated alumina compared to untreated alumina has been reported by Roscoe and Abbatt (2005). The enhanced ice nucleation activity of LE-Ka observed here could be due to water adsorption on the alumina rich (40 % by mass) particle surface given that water vapour molecules play a key role in the deposition ice nucleation. For immersion mode, the particles instantaneously activate to liquid droplets upon entering IMCA therefore water vapour adsorption is not relevant. The smaller enhancement of LE-Ka in the immersion mode (Fig. 11a) relative to deposition nucleation is therefore

ACPD
13, 8701–8767, 2013

expected and could be due to a surface oxide (M=O) species resulting from ozone exposure providing active sites for stabilisation of liquid water clusters.

ATD responded differently to the O_3 exposure in both deposition and immersion mode, i.e. no significant enhancement in ice formation was observed. This is not surprising however given that the BET surface area of ATD is 50 % that of Ka and thus presents a smaller surface area that can be altered due to heterogeneous oxidation of O_3. Compared to Ka, ATD is composed on average of only ∼12 % (by mass) alumina. We can thus expect fewer surface oxide species to form. Inferring from the ozone coverage of the ATD (in Table 1) which is an order of magnitude higher than that reported to be the maximum saturated coverage for MD (see Sect. 4.1), we conclude catalytic destruction of O_3 on the ATD surface sites. An O_2 molecule is likely released per site regenerating the surface sites with little to no change of the surface at the O_3 concentrations used here (Cwiertny et al., 2008).

4.3.2 Effect of high O_3 exposure

The HE particles showed reduced ice nucleation activity compared to untreated particles in the deposition mode. For HE-Ka the suppression was observed for $230 < T < 240$ K by approximately an order of magnitude, whereas for HE-ATD the suppression was lower and observed for the entire T range studied. At first glance the suppression observed in both Ka and ATD is counter intuitive since one could expect that a higher O_3 exposure should result in larger enhancement in AF than the low O_3 exposure experiments, assuming a linear relation. However in context of O_3 uptake measurements on MD reported in the literature (Hanisch and Crowley, 2003), we suggest an explanation for the observed suppression of IN ability. Hanish and Crowley (2003) reported that O_3 can bind to MD surfaces in both reactive and unreactive configurations and that non-reactively bound O_3 will result in blocking reactive O_3 sites. This is thought to particularly occur at higher O_3 concentrations such as those used for our HE experiments. We propose that blocked sites are unable to catalyse water adsorption as occurs in the LE experiments. The weaker suppression exhibited by HE-ATD is

ACPD
13, 8701–8767, 2013

expected due to the lower number of surface sites available for heterogeneous uptake of O_3 indicated by the lower BET surface area, reflecting the different surface compositions of Ka and ATD.

For immersion freezing HE-ATD showed a larger suppression in n_s than HE-Ka. A reason could be due blocked reactive sites on the surface if ATD that are likely ice nucleation active sites arsing from the physisorption of O_3 that occurs on silica (Usher et al., 2003a) at high concentrations through non-reactive O_3 binding (Hanisch and Crowley, 2003). This behaviour would be pronounced in ATD since it is composed of ~ 75 % (by mass) of silica, whereas Ka is only 40 % (by mass) silica. This would be true if the condensation of water onto the HE-Ka particles prior to freezing, results in the dissociation of the O_3 from the blocked surface sites whereas the same is not occurring with ATD either due to the different surface composition or the higher O_3 concentrations for the HE-ATD experiments.

4.4 Limitations

The surrogates of atmospheric MD used here are not replicates of the atmospheric dust. Despite the minimal processing involved in producing the Ka particles used here, it is a single component clay. On the other hand, ATD is representative of a natural dust composition (complex mixture), but undergoes significant milling and drying in its production process which likely results in it being artificially enhanced as an IN compared to natural desert dusts. Nevertheless, this work shows that there is an effect of O_3 exposure on the dust particles and future such studies can focus on natural desert dust particles or other clay minerals such as illite.

As discussed at the end of Sect. 4.1, the typical O_3 concentrations in the troposphere are an order of magnitude lower than those used in the current work for our low exposure studies. This could result in lower surface coverage in the atmosphere and thus the extent to which IN properties are altered could vary from what we present here. However, this work shows that there is an O_3 concentration effect on the IN properties and it would be necessary to conduct studies at lower concentrations.

ACPD
13, 8701–8767, 2013

Lastly, we use the spherical assumption for geometric surface area to be consistent when comparing the outcome of IN concentrations from the $n_s(T)$ parameterizations to those from the field studies (presented in Sect. 6) because surface areas estimated from the field studies are also based on geometrical surface areas. This also ensures consistency when comparing our $n_s(T)$ to previous studies. The BET surface area may over estimate the surface available to a water molecule adsorbing to the surface of a MD particle because of the partly hydrophobic nature of MD particles, thus one can expect that a smaller area is available to water molecules than the surface occupied by N_2 for BET measurements (Zettlemoyer et al., 1961). Additionally, we assume that the particle composition across different sizes is uniform, which is not true for ATD submicron particle composition compared to the bulk (Vlasenko et al., 2005). However we note that the particles used here are all in the submicron size range.

4.5 Comparison to previous work

This is one of the first studies to show an inhibition of ice nucleation explicitly in the immersion regime due to ageing of dust particles at atmospherically relevant conditions. A study by Sullivan et al. (2010b) reports enhanced loss of IN activity of sulphuric acid coated ATD particles in the condensation – immersion regime, however the particles were heated during the coating process to $45\,^{\circ}\mathrm{C} < T < 85\,^{\circ}\mathrm{C}$ and the authors report that the effect of heating-coating combination could not be separated from that of coating (ageing) alone.

There has been one previous study that investigated the influence on ice nucleation of ageing montmorillonite at 200 ppbv O_3 for $233 < T < 258$ K (Salam et al., 2008). In the study, a CFDC was used to detect deposition mode ice nucleation and results reported for AF at $RH_w = 90\,\%$ showed no difference in IN activity between O_3 aged and untreated montmorillonite particles. This is contrary to what we observe in the deposition mode for aged Ka. Reasons for this could be numerous. First, we observe in the current work that IN properties of ATD and Ka do not respond to O_3 ageing in the same manner, therefore it is not surprising that an ageing effect was not

ACPD
13, 8701–8767, 2013

observed in the deposition mode for montmorillonite, similar to what we observe for LE-ATD in this work. Second, only one concentration of O_3 (200 ppbv) was applied in the Salam et al. (2008) study, which is less than half the concentration we used for the low exposure studies. Third, ageing times were significantly different, 70 h in the Salam et al. (2008) study and ~ 2 h in the current work. To date there are no additional studies that have investigated the ice nucleation properties of dust aged with O_3. A number of studies discussed in the literature have looked at IN effects from ageing through condensing inorganic or organic coatings onto MD particles and have found a reduced efficiency of ice nucleation (see Sect. 2). We note that in general internally mixed MD particles with typical atmospheric ageing proxies, result in suppression or no change in ice nucleation behaviour when compared to the corresponding bare MD particles, similar to what has been observed here with the HE-Ka and HE-ATD.

The parameterisation for $n_s(T)$ from the work of Niemand et al. (2012) derived from fitting collectively the immersion mode freezing $n_s(T)$ for natural untreated dust samples including Asian dust, Canary Island dust, Israeli dust and Saharan dust is plotted in Fig. 11. Their parameterisation fit is based on data obtained in the T range 258 to 238 K. We plot this parameterisation and extrapolate it to 232 K to compare to the n_s derived in this work. It is evident that the natural dusts have n_s that are comparable to that of Ka particularly at $T > 240$ K. This parameterisation suggests that the Ka particles used here from Clay Mineral Society could be a good representative of natural dust particles, contrary to what is observed in Fig. 11b where the natural dust n_s at $T > 235$ K are significantly lower than that of ATD. What is striking is that the natural dust fit is significantly lower than the already suppressed n_s of HE-ATD lending support to the active IN nature of ATD compared to other MD species (Murray et al., 2012) attributed to the manufacturing process of ATD.

ACPD
13, 8701–8767, 2013

5 Atmospheric implications

The observations of ice active fraction as a function of temperature presented in this work show that MD particles' ice nucleation properties will be altered as a result of heterogeneous oxidation with O_3. It should be noted that the concentrations used here are higher than typical concentrations found in the atmosphere, except in some cases as discussed at the end of Sect. 4.1. The enhancement observed in the ice nucleation capability of Ka due to moderate ageing with O_3 could result in increased heterogeneous ice formation. It has been shown using box model simulations that the presence of efficient IN will suppress the initiation of homogeneous ice nucleation events, especially in the presence of high IN concentrations of which desert dust plumes are an example (Spichtinger and Cziczo, 2010).

In this work we also observe O_3 loss to both Ka and ATD surfaces implying that MD is a sink for O_3. The findings of ozone uptake presented here are in agreement with previous works that have studied the process with a detailed focus on kinetics and uptake mechanism. In particular the study by Dentener et al. (1996) reports that uptake coefficients of at least 10^{-5} are required for the heterogeneous reaction of O_3 to be considered an important loss pathway in the atmosphere. This magnitude is observed for the loss to both Ka and ATD in the current work (Table 1).

In order to assess the significance of the ice nucleation results presented here, we use the derived parameterisations for Ka (immersion mode), which shows the better match to natural desert dust IN activity, to demonstrate relevance of this laboratory work to the atmosphere. The following assessment is relevant for regions of the troposphere where the updraft velocities are high enough, for example the upper tropical troposphere (Lohmann and Feichter, 2005) such that ice formation is largely dependent on temperature. To make the connection to the atmosphere, we estimate the potential concentration of atmospheric IN using $n_s(T)$ for Ka and LE-KA for immersion mode from Table 6 at 248 K to be 3.6×10^9 sites m^{-2} and 6.0×10^9 sites m^{-2}, respectively. Estimates of the surface area concentration of potential aerosol particles that can

ACPD
13, 8701–8767, 2013

nucleate ice in the atmosphere are calculated using the range in Murray et al. (2012) for dust, 50–0.1 particles cm^{-3}. Assuming d = 1 µm and spherical particles, the surface area available for potential ice nucleation is 1.6×10^{-10} to 3.1×10^{-13} $m^{-2}\,cm^{-3}$. The potential IN concentrations can then be estimated according to:

$$[IN]_{248\,K}\left(\#\,cm^{-3}\right) = n_s\,(248\,K)\left(sites\,m^{-2}\right) \times SA_{tot}\left(m^{-2}\,cm^{-3}\right) \quad (5)$$

We find that the IN concentrations would be on the order of 10^{-1}–10^{-3} cm^{-3} and 10–10^{-2} cm^{-3} for particles that have IN properties similar to Ka and LE-Ka in the immersion mode, respectively. The range of IN concentrations derived from the Ka parameterisation here agree extremely well with the potential atmospheric IN concentrations reported in Murray et al. (2012) for natural desert dusts.

During the CRYSTAL-FACE campaign, DeMott et al. (2003b) report peak IN concentrations of up to 1–2 cm^{-3} during the dust storm detected using an IN counter in the deposition mode at RH_w = 86 % and T = 236 K. From the data presented in the paper, we estimate the surface area present during the dust storm to be 3×10^{-6} $cm^2\,cm^{-3}$, which is similar to the surface area of 1.6×10^{-6} $cm^2\,cm^{-3}$ reported for another Saharan dust storm event (de Reus et al., 2000). If we determine n_s(236 K) from our deposition mode parameterizations of Ka from Table 5, we get 3.3×10^9 sites m^{-2}. Using Eq. (5) we predict an IN concentration of 1 cm^{-3}. This is in remarkably good agreement between the extrapolation of a laboratory study and a field measurement given instrument uncertainties. We also note that during CRYSTAL-FACE, MD residuals from ice crystals were found to be bare and not internally mixed with sulphate or organics. Lastly, in a study called PACDEX (Stith et al., 2009), IN concentrations of 6 L^{-1} were observed in a dust plume being transported from Asia over the Pacific Ocean to a longitude of 139° and an altitude between 12.5 and 13.3 km and were measured in the T range 237–241 K using an IN counter at water saturation. From these data, the surface area concentration of the particles at the same location in the plume is estimated to be 4.2×10^{-7} $cm^2\,cm^{-3}$. If we assume that due to long range transport, these particles are aged for times similar to the HE-Ka, we can use the deposition mode data of

ACPD
13, 8701–8767, 2013

HE-Ka for $n_s(239\,\mathrm{K}) = 1 \times 10^{-11}$ sites m^{-2} (Fig. 10a) which results in an IN concentration of 4.2 L^{-1}. This is less than a factor of two apart from the measured value in the dust plume. We note again that our estimate of IN concentrations in the atmosphere is based on a parameterisation at $RH_w = 95\,\%$ while the measurements are conducted at 100 %, expecting the higher measured concentration than the predicted value. To conclude, we note that the conditions of the field study guide our choice of which parameterisation to use for this comparison. For example, using the parameterisation for untreated Ka or LE-Ka would not result in good agreement between measured and predicted values in the above examples.

6 Conclusions

The ice nucleation properties of two mineral dust particle types, kaolinite (KGa-1b) and Arizona Test Dust at temperatures relevant to the heterogeneous freezing regime ($T > 233$ K) for deposition and immersion mode ice nucleation at different exposure levels of chemical ageing due to ozone (0.43 ppmv for Ka and ATD, 1.4 ppmv for Ka and 4.3 ppmv for ATD). We present parameterisations of ice active fractions and ice active surface densities as a function of temperature for both ice nucleation modes that can be used for comparison to other studies and for implementation in ice nucleation modelling work. This is the first study to show the enhancement of IN activity of mineral dust particles due to atmospherically relevant O_3 chemical ageing for both deposition and immersion mode ice nucleation. For ageing times of ~ 130 min and ozone concentrations of ~ 430 ppbv, equivalent to particles exposed to typical tropospheric background ozone concentrations of 45 ppbv for 1 day, we found that aged kaolinite particles showed enhanced ice nucleation activity compared to untreated kaolinite in the deposition and immersion mode in the temperature range studied here (264–233 K). For the same level of ozone ageing Arizona Test Dust showed a small, quantitatively indistinguishable enhancement of ice nucleation activity (based on n_s) for both deposition and immersion ice nucleation. Uptake coefficients (γ) determined for the above

ACPD
13, 8701–8767, 2013

ageing experiments were found to be on the order of 10^{-5} and 10^{-4} for kaolinite and Arizona Test Dust respectively which are in agreement with previous values reported in the literature. Kaolinite particles aged for ~130 min at 1.4 ppmv corresponding to ~3 days of atmospheric exposure at 45 ppbv showed a lower ice nucleation activity in the temperature range 232–240 K compared to untreated kaolinite in the deposition mode. In the immersion mode only a small suppression of ice active surface sites was found for the temperature range presented here. Arizona Test Dust particles aged for the same time at 4.3 ppmv ozone corresponding to ~9 days atmospheric exposure, showed a significantly lower ice nucleation compared to untreated Arizona Test Dust in the deposition mode across the entire temperature range studied. In the immersion mode, the same particles were found to have up to and an order of magnitude lower ice active surface sites in the investigated temperature range.

Based on an ice active surface site density parameterisation, we show that Arizona Test Dust is found to have significantly higher ice nucleation activity compared to kaolinite and natural desert dusts. Parameterisations derived for kaolinite were used to predict ice nuclei concentrations measured in the atmosphere. We find good agreement with previous values reported from field measurements of ice nuclei concentrations conducted inside dust plumes. We also suggest that the kaolinite sample used here (KGa-1b) from Clay Mineral Society is a better surrogate for natural desert dusts than Arizona Test Dust. While using ice active site densities is a convenient way of comparing ice nucleation data across different modes, sample types and instruments, it should be noted that particle size effects (due to non-uniform composition across varying particle sizes), and time can still transcend this representation, in particular for particles with diameters less than 100 nm where the probability occurrence of an ice active site is very low (Kanji and Abbatt, 2010). To extrapolate these results to regions in the atmosphere where ice nucleation results from small cooling rates, it would be beneficial to include a time dependent parameterization based on classical nucleation theory (e.g. Welti et al., 2012; Murray et al., 2011).

ACPD
13, 8701–8767, 2013

In conclusion we observe non-uniform and non-linear responses in ice nucleation to ozone ageing of kaolinite and Arizona Test Dust particles for low and high effective ozone ageing times in both immersion and deposition mode ice nucleation. Quantitatively, based on ice active surface site densities, deposition mode was significantly affected by the ageing experiments, thus similar studies would be desirable at temperatures relevant to the cirrus regime ($T < 233$ K) where deposition mode is more important. In order to better understand the processes of ageing and their effects on ice nucleation, similar experiments with other trace gases such as NO_2 and SO_2 should be performed with a variety of atmospherically relevant mineral particles and potentially with monodisperse particle populations. Systematic investigations of the response of ice nuclei varying ageing gas concentrations are desirable to explore the potential mechanisms of enhancing or suppressing the ice nucleation efficiency of mineral dusts.

Acknowledgements. The authors would like to acknowledge Hannes Wydler for technician support and funding from the Swiss National Science Foundation (SNSF) project contract number 200021_127275, "Laboratory and Field Studies of Ice Nucleation: Natural and Anthropogenic Effects".

References

Abbatt, J. P. D.: Interactions of atmospheric trace gases with ice surfaces: adsorption and reaction, Chem. Rev., 103, 4783–4800, doi:10.1021/cr0206418, 2003.

Alpert, P. A., Aller, J. Y., and Knopf, D. A.: Ice nucleation from aqueous NaCl droplets with and without marine diatoms, Atmos. Chem. Phys., 11, 5539–5555, doi:10.5194/acp-11-5539-2011, 2011.

Andreae, M. O. and Rosenfeld, D.: Aerosol-cloud-precipitation interactions. Part I: the nature and sources of cloud-active aerosols, Earth-Sci. Rev., 89, 13–41, doi:10.1016/j.earscirev.2008.03.001, 2008.

Archuleta, C. M., DeMott, P. J., and Kreidenweis, S. M.: Ice nucleation by surrogates for atmospheric mineral dust and mineral dust/sulfate particles at cirrus temperatures, Atmos. Chem. Phys., 5, 2617–2634, doi:10.5194/acp-5-2617-2005, 2005.

ACPD
13, 8701–8767, 2013

Baustian, K. J., Cziczo, D. J., Wise, M. E., Pratt, K. A., Kulkarni, G., Hallar, A. G., and Tolbert, M. A.: Importance of aerosol composition, mixing state, and morphology for heterogeneous ice nucleation: a combined field and laboratory approach, J. Geophys. Res.-Atmos., 117, D06217, doi:10.1029/2011jd016784, 2012.

Cantrell, W. and Heymsfield, A.: Production of ice in tropospheric clouds – a review, B. Am. Meteorol. Soc., 86, 795–807, doi:10.1175/bams-86-6-795, 2005.

Chang, R. Y. W., Sullivan, R. C., and Abbatt, J. P. D.: Initial uptake of ozone on Saharan dust at atmospheric relative humidities, Geophys. Res. Lett., 32, L14815, doi:10.1029/2005gl023317, 2005.

Chou, C., Stetzer, O., Weingartner, E., Jurányi, Z., Kanji, Z. A., and Lohmann, U.: Ice nuclei properties within a Saharan dust event at the Jungfraujoch in the Swiss Alps, Atmos. Chem. Phys., 11, 4725–4738, doi:10.5194/acp-11-4725-2011, 2011.

Chou, C., Kanji, Z. A., Stetzer, O., Tritscher, T., Chirico, R., Heringa, M. F., Weingartner, E., Prévôt, A. S. H., Baltensperger, U., and Lohmann, U.: Effect of photochemical ageing on the ice nucleation properties of diesel and wood burning particles, Atmos. Chem. Phys., 13, 761–772, doi:10.5194/acp-13-761-2013, 2013.

Colarco, P. R., Toon, O. B., Reid, J. S., Livingston, J. M., Russell, P. B., Redemann, J., Schmid, B., Maring, H. B., Savoie, D., Welton, E. J., Campbell, J. R., Holben, B. N., and Levy, R.: Saharan dust transport to the Caribbean during PRIDE: 2. Transport, vertical profiles, and deposition in simulations of in situ and remote sensing observations, J. Geophys. Res.-Atmos., 108, 8590, doi:10.1029/2002jd002659, 2003.

Connolly, P. J., Möhler, O., Field, P. R., Saathoff, H., Burgess, R., Choularton, T., and Gallagher, M.: Studies of heterogeneous freezing by three different desert dust samples, Atmos. Chem. Phys., 9, 2805–2824, doi:10.5194/acp-9-2805-2009, 2009.

Cwiertny, D. M., Young, M. A., and Grassian, V. H.: Chemistry and photochemistry of mineral dust aerosol, in: Annu. Rev. Phys. Chem., 59, 27–51, 2008.

Cziczo, D. J., Murphy, D. M., Hudson, P. K., and Thomson, D. S.: Single particle measurements of the chemical composition of cirrus ice residue during crystal-face, J. Geophys. Res.-Atmos., 109, D04201, doi:10.1029/2003JD004032, 2004.

Cziczo, D. J., Froyd, K. D., Gallavardin, S. J., Moehler, O., Benz, S., Saathoff, H., and Murphy, D. M.: Deactivation of ice nuclei due to atmospherically relevant surface coatings, Environ. Res. Lett., 4, 044013, doi:10.1088/1748-9326/4/4/044013, 2009.

ACPD
13, 8701–8767, 2013

de Reus, M., Dentener, F., Thomas, A., Borrmann, S., Strom, J., and Lelieveld, J.: Airborne observations of dust aerosol over the North Atlantic Ocean during ACE 2: indications for heterogeneous ozone destruction, J. Geophys. Res.-Atmos., 105, 15263–15275, 2000.

DeMott, P. J., Cziczo, D. J., Prenni, A. J., Murphy, D. M., Kreidenweis, S. M., Thomson, D. S., Borys, R., and Rogers, D. C.: Measurements of the concentration and composition of nuclei for cirrus formation, P. Natl. Acad. Sci. USA, 100, 14655–14660, 2003a.

DeMott, P. J., Sassen, K., Poellot, M. R., Baumgardner, D., Rogers, D. C., Brooks, S. D., Prenni, A. J., and Kreidenweis, S. M.: African dust aerosols as atmospheric ice nuclei, Geophys. Res. Lett., 30, 1732, doi:10.1029/2003GL017410, 2003b.

DeMott, P. J., Petters, M. D., Prenni, A. J., Carrico, C. M., Kreidenweis, S. M., Collett, J. L., and Moosmuller, H.: Ice nucleation behavior of biomass combustion particles at cirrus temperatures, J. Geophys. Res.-Atmos., 114, D16205, doi:10.1029/2009JD012036, 2009.

DeMott, P. J., Prenni, A. J., Liu, X., Kreidenweis, S. M., Petters, M. D., Twohy, C. H., Richardson, M. S., Eidhammer, T., and Rogers, D. C.: Predicting global atmospheric ice nuclei distributions and their impacts on climate, P. Natl. Acad. Sci. USA, 107, 11217–11222, doi:10.1073/pnas.0910818107, 2010.

Denman, K. L., Brasseur, G., Chidthaisong, A., Ciais, P., Cox, P. M., Dickinson, R. E., Hauglustaine, D., Heinze, C., Holland, E., Jacob, D., Lohmann, U., Ramachandran, S., Dias, P. L. D. S., Wofsy, S. C., and Zhang, X.: Couplings between changes in the climate system and biogeochemistry, in: Climate Change 2007: The Physical Science Basis. Contribution of Working Group I to the Fourth Assessment Report of the Intergovernmental Panel on Climate Change edited by: Solomon, S., Qin, D., Manning, M., Chen, Z., Marquis, M., Averyt, K. B., Tignor, M. and Miller, H. L., Cambridge University Press, Cambridge, UK and New York, NY, USA, 2007.

Dentener, F. J., Carmichael, G. R., Zhang, Y., Lelieveld, J., and Crutzen, P. J.: Role of mineral aerosol as a reactive surface in the global troposphere, J. Geophys. Res.-Atmos., 101, 22869–22889, 1996.

Diehl, K. and Wurzler, S.: Heterogeneous drop freezing in the immersion mode: model calculations considering soluble and insoluble particles in the drops, J. Atmos. Sci., 61, 2063–2072, doi:10.1175/1520-0469(2004)061<2063:hdfiti>2.0.co;2, 2004.

Earle, M. E., Kuhn, T., Khalizov, A. F., and Sloan, J. J.: Volume nucleation rates for homogeneous freezing in supercooled water microdroplets: results from a combined experimental

ACPD
13, 8701–8767, 2013

and modelling approach, Atmos. Chem. Phys., 10, 7945–7961, doi:10.5194/acp-10-7945-2010, 2010.
Eastwood, M. L., Cremel, S., Wheeler, M., Murray, B. J., Girard, E., and Bertram, A. K.: Effects of sulfuric acid and ammonium sulfate coatings on the ice nucleation properties of kaolinite particles, Geophys. Res. Lett., 36, L02811, doi:10.1029/2008gl035997, 2009.
Eidhammer, T., DeMott, P. J., and Kreidenweis, S. M.: A comparison of heterogeneous ice nucleation parameterizations using a parcel model framework, J. Geophys. Res.-Atmos., 114, D06202, doi:10.1029/2008jd011095, 2009.
Field, P. R., Heymsfield, A. J., Shipway, B. J., DeMott, P. J., Pratt, K. A., Rogers, D. C., Stith, J., and Prather, K. A.: Ice in clouds experiment-layer clouds. Part II: Testing characteristics of heterogeneous ice formation in lee wave clouds, J. Atmos. Sci., 69, 1066–1079, doi:10.1175/jas-d-11-026.1, 2012.
Hanisch, F. and Crowley, J. N.: Ozone decomposition on Saharan dust: an experimental investigation, Atmos. Chem. Phys., 3, 119–130, doi:10.5194/acp-3-119-2003, 2003.
Hoose, C. and Möhler, O.: Heterogeneous ice nucleation on atmospheric aerosols: a review of results from laboratory experiments, Atmos. Chem. Phys., 12, 9817–9854, doi:10.5194/acp-12-9817-2012, 2012.
Hung, H. M., Malinowski, A., and Martin, S. T.: Kinetics of heterogeneous ice nucleation on the surfaces of mineral dust cores inserted into aqueous ammonium sulfate particles, J. Phys. Chem. A, 107, 1296–1306, 2003.
Kanji, Z. A. and Abbatt, J. P. D.: Laboratory studies of ice formation via deposition mode nucleation onto mineral dust and n-hexane soot samples, J. Geophys. Res.-Atmos., 111, D16204, doi:10.1029/2005JD006766, 2006.
Kanji, Z. A. and Abbatt, J. P. D.: Ice nucleation onto arizona test dust at cirrus temperatures: effect of temperature and aerosol size on onset relative humidity, J. Phys. Chem. A, 114, 935–941, doi:10.1021/jp908661m, 2010.
Kanji, Z. A., Florea, O., and Abbatt, J. P. D.: Ice formation via deposition nucleation on mineral dust and organics: dependence of onset relative humidity on total particulate surface area, Environ. Res. Lett, 3, 025004, doi:10.1088/1748-9326/3/2/025004, 2008.
Kanji, Z. A., DeMott, P. J., Möhler, O., and Abbatt, J. P. D.: Results from the University of Toronto continuous flow diffusion chamber at ICIS 2007: instrument intercomparison and ice onsets for different aerosol types, Atmos. Chem. Phys., 11, 31–41, doi:10.5194/acp-11-31-2011, 2011.

ACPD
13, 8701–8767, 2013

Karagulian, F. and Rossi, M. J.: The heterogeneous decomposition of ozone on atmospheric mineral dust surrogates at ambient temperature, Int. J. Chem. Kinet., 38, 407–419, doi:10.1002/kin.20175, 2006.
Knopf, D. A., Wang, B., Laskin, A., Moffet, R. C., and Gilles, M. K.: Heterogeneous nucleation of ice on anthropogenic organic particles collected in Mexico City, Geophys. Res. Lett., 37, L11803, doi:10.1029/2010gl043362, 2010.
Knopf, D. A., Alpert, P. A., Wang, B., and Aller, J. Y.: Stimulation of ice nucleation by marine diatoms, Nat. Geosci., 4, 88–90, doi:10.1038/ngeo1037, 2011.
Koehler, K. A., Kreidenweis, S. M., DeMott, P. J., Prenni, A. J., and Petters, M. D.: Potential impact of Owens (dry) Lake dust on warm and cold cloud formation, J. Geophys. Res.-Atmos., 112, D12210, doi:10.1029/2007JD008413, 2007.
Koehler, K. A., Kreidenweis, S. M., DeMott, P. J., Petters, M. D., Prenni, A. J., and Carrico, C. M.: Hygroscopicity and cloud droplet activation of mineral dust aerosol, Geophys. Res. Lett., 36, L08805, doi:10.1029/2009gl037348, 2009.
Kolb, C. E., Cox, R. A., Abbatt, J. P. D., Ammann, M., Davis, E. J., Donaldson, D. J., Garrett, B. C., George, C., Griffiths, P. T., Hanson, D. R., Kulmala, M., McFiggans, G., Pöschl, U., Riipinen, I., Rossi, M. J., Rudich, Y., Wagner, P. E., Winkler, P. M., Worsnop, D. R., and O' Dowd, C. D.: An overview of current issues in the uptake of atmospheric trace gases by aerosols and clouds, Atmos. Chem. Phys., 10, 10561–10605, doi:10.5194/acp-10-10561-2010, 2010.
Koop, T., Luo, B. P., Tsias, A., and Peter, T.: Water activity as the determinant for homogeneous ice nucleation in aqueous solutions, Nature, 406, 611–614, 2000.
Ladino, L., Stetzer, O., Luond, F., Welti, A., and Lohmann, U.: Contact freezing experiments of kaolinite particles with cloud droplets, J. Geophys. Res.-Atmos., 116, D22202, doi:10.1029/2011jd015727, 2011.
Li, W. and Oyama, S. T.: Mechanism of ozone decomposition on a manganese oxide catalyst. 2. Steady-state and transient kinetic studies, J. Am. Chem. Soc., 120, 9047–9052, doi:10.1021/ja9814422, 1998.
Li, W., Gibbs, G. V., and Oyama, S. T.: Mechanism of ozone decomposition on a manganese oxide catalyst. I. In situ Raman spectroscopy and ab initio molecular orbital calculations, J. Am. Chem. Soc., 120, 9041–9046, doi:10.1021/ja981441+, 1998.
Li, W. J. and Shao, L. Y.: Observation of nitrate coatings on atmospheric mineral dust particles, Atmos. Chem. Phys., 9, 1863–1871, doi:10.5194/acp-9-1863-2009, 2009.

ACPD
13, 8701–8767, 2013

Lindzen, R. S.: Some coolness concerning global warming, B. Am. Meteorol. Soc., 71, 288–299, 1990.
Lohmann, U. and Feichter, J.: Global indirect aerosol effects: a review, Atmos. Chem. Phys., 5, 715–737, doi:10.5194/acp-5-715-2005, 2005.
Lüönd, F., Stetzer, O., Welti, A., and Lohmann, U.: Experimental study on the ice nucleation ability of size-selected kaolinite particles in the immersion mode, J. Geophys. Res.-Atmos., 115, D14201, doi:10.1029/2009jd012959, 2010.
Marcolli, C., Gedamke, S., Peter, T., and Zobrist, B.: Efficiency of immersion mode ice nucleation on surrogates of mineral dust, Atmos. Chem. Phys., 7, 5081–5091, doi:10.5194/acp-7-5081-2007, 2007.
Michel, A. E., Usher, C. R., and Grassian, V. H.: Heterogeneous and catalytic uptake of ozone on mineral oxides and dusts: a Knudsen cell investigation, Geophys. Res. Lett., 29, 1665, doi:10.1029/2002gl014896, 2002.
Michel, A. E., Usher, C. R., and Grassian, V. H.: Reactive uptake of ozone on mineral oxides and mineral dusts, Atmos. Environ., 37, 3201–3211, doi:10.1016/s1352-2310(03)00319-4, 2003.
Mogili, P. K., Kleiber, P. D., Young, M. A., and Grassian, V. H.: Heterogeneous uptake of ozone on reactive components of mineral dust aerosol: an environmental aerosol reaction chamber study, J. Phys. Chem. A, 110, 13799–13807, doi:10.1021/jp063620g, 2006.
Möhler, O., DeMott, P. J., Vali, G., and Levin, Z.: Microbiology and atmospheric processes: the role of biological particles in cloud physics, Biogeosciences, 4, 1059–1071, doi:10.5194/bg-4-1059-2007, 2007.
Möhler, O., Benz, S., Saathoff, H., Schnaiter, M., Wagner, R., Schneider, J., Walter, S., Ebert, V., and Wagner, S.: The effect of organic coating on the heterogeneous ice nucleation efficiency of mineral dust aerosols, Environ. Res. Lett., 3, 025007, doi:10.1088/1748-9326/3/2/025007, 2008.
Murray, B. J., Broadley, S. L., Wilson, T. W., Atkinson, J. D., and Wills, R. H.: Heterogeneous freezing of water droplets containing kaolinite particles, Atmos. Chem. Phys., 11, 4191–4207, doi:10.5194/acp-11-4191-2011, 2011.
Murray, B. J., O'Sullivan, D., Atkinson, J. D., and Webb, M. E.: Ice nucleation by particles immersed in supercooled cloud droplets, Chem. Soc. Rev., 41, 6519–6554, doi:10.1039/c2cs35200a, 2012.

ACPD
13, 8701–8767, 2013

Nicolet, M., Stetzer, O., Lüönd, F., Möhler, O., and Lohmann, U.: Single ice crystal measurements during nucleation experiments with the depolarization detector IODE, Atmos. Chem. Phys., 10, 313–325, doi:10.5194/acp-10-313-2010, 2010.

Niedermeier, D., Hartmann, S., Shaw, R. A., Covert, D., Mentel, T. F., Schneider, J., Poulain, L., Reitz, P., Spindler, C., Clauss, T., Kiselev, A., Hallbauer, E., Wex, H., Mildenberger, K., and Stratmann, F.: Heterogeneous freezing of droplets with immersed mineral dust particles – measurements and parameterization, Atmos. Chem. Phys., 10, 3601–3614, doi:10.5194/acp-10-3601-2010, 2010.

Niedermeier, D., Hartmann, S., Clauss, T., Wex, H., Kiselev, A., Sullivan, R. C., DeMott, P. J., Petters, M. D., Reitz, P., Schneider, J., Mikhailov, E., Sierau, B., Stetzer, O., Reimann, B., Bundke, U., Shaw, R. A., Buchholz, A., Mentel, T. F., and Stratmann, F.: Corrigendum to "Experimental study of the role of physicochemical surface processing on the IN ability of mineral dust particles" published in Atmos. Chem. Phys., 11, 11131–11144, 2011, Atmos. Chem. Phys., 11, 11919–11919, doi:10.5194/acp-11-11919-2011, 2011a.

Niedermeier, D., Hartmann, S., Clauss, T., Wex, H., Kiselev, A., Sullivan, R. C., DeMott, P. J., Petters, M. D., Reitz, P., Schneider, J., Mikhailov, E., Sierau, B., Stetzer, O., Reimann, B., Bundke, U., Shaw, R. A., Buchholz, A., Mentel, T. F., and Stratmann, F.: Experimental study of the role of physicochemical surface processing on the IN ability of mineral dust particles, Atmos. Chem. Phys., 11, 11131–11144, doi:10.5194/acp-11-11131-2011, 2011b.

Niemand, M., Mohler, O., Vogel, B., Vogel, H., Hoose, C., Connolly, P., Klein, H., Bingemer, H., DeMott, P., Skrotzki, J., and Leisner, T.: A particle-surface-area-based parameterization of immersion freezing on desert dust particles, J. Atmos. Sci., 69, 3077–3092, doi:10.1175/jas-d-11-0249.1, 2012.

Pinti, V., Marcolli, C., Zobrist, B., Hoyle, C. R., and Peter, T.: Ice nucleation efficiency of clay minerals in the immersion mode, Atmos. Chem. Phys., 12, 5859–5878, doi:10.5194/acp-12-5859-2012, 2012.

Pratt, K. A., DeMott, P. J., French, J. R., Wang, Z., Westphal, D. L., Heymsfield, A. J., Twohy, C. H., Prenni, A. J., and Prather, K. A.: In situ detection of biological particles in cloud ice-crystals, Nat. Geosci., 2, 397–400, doi:10.1038/ngeo521, 2009.

Prospero, J. M.: Long-range transport of mineral dust in the global atmosphere: impact of African dust on the environment of the southeastern United States, P. Natl. Acad. Sci. USA, 96, 3396–3403, 1999.

ACPD
13, 8701–8767, 2013

Pruppacher, H. R. and Klett, J. D.: Microphysics of Clouds and Precipitation, 2nd edn., Kluwer, Dordrecht, 976 pp., 1997.
Richardson, M. S., DeMott, P. J., Kreidenweis, S. M., Cziczo, D. J., Dunlea, E. J., Jimenez, J. L., Thomson, D. S., Ashbaugh, L. L., Borys, R. D., Westphal, D. L., Casuccio, G. S., and Lersch, T. L.: Measurements of heterogeneous ice nuclei in the western United States in springtime and their relation to aerosol characteristics, J. Geophys. Res.-Atmos., 112, D02209, doi:10.1029/2006jd007500, 2007.
Rogers, D. C.: Development of a continuous flow thermal gradient diffusion chamber for ice nucleation studies, Atmos. Res., 22, 149–181, doi:10.1016/0169-8095(88)90005-1, 1988.
Roscoe, J. M. and Abbatt, J. P. D.: Diffuse reflectance FTIR study of the interaction of alumina surfaces with ozone and water vapor, J. Phys. Chem. A, 109, 9028–9034, doi:10.1021/jp050766r, 2005.
Salam, A., Lohmann, U., Crenna, B., Lesins, G., Klages, P., Rogers, D., Irani, R., MacGillivray, A., and Coffin, M.: Ice nucleation studies of mineral dust particles with a new continuous flow diffusion chamber, Aerosol Sci. Tech., 40, 134–143, doi:10.1080/02786820500444853, 2006.
Salam, A., Lesins, G., and Lohmann, U.: Laboratory study of heterogeneous ice nucleation in deposition mode of montmorillonite mineral dust particles aged with ammonia, sulfur dioxide, and ozone at polluted atmospheric concentrations, Air Qual. Atmos. Health, 1, 135–142, doi:10.1007/s11869-008-0019-6, 2008.
Sassen, K., DeMott, P. J., Prospero, J. M., and Poellot, M. R.: Saharan dust storms and indirect aerosol effects on clouds: CRYSTAL-FACE results, Geophys. Res. Lett., 30, 1633, doi:10.1029/2003GL017371, 2003.
Satheesh, S. K. and Moorthy, K. K.: Radiative effects of natural aerosols: a review, Atmos. Environ., 39, 2089–2110, doi:10.1016/j.atmosenv.2004.12.029, 2005.
Spichtinger, P. and Cziczo, D. J.: Impact of heterogeneous ice nuclei on homogeneous freezing events in cirrus clouds, J. Geophys. Res.-Atmos., 115, D14208, doi:10.1029/2009jd012168, 2010.
Stetzer, O., Baschek, B., Luond, F., and Lohmann, U.: The Zurich Ice Nucleation Chamber (ZINC) – a new instrument to investigate atmospheric ice formation, Aerosol Sci. Tech.,A 42, 64–74, doi:10.1080/02786820701787944, 2008.
Stith, J. L., Ramanathan, V., Cooper, W. A., Roberts, G. C., DeMott, P. J., Carmichael, G., Hatch, C. D., Adhikary, B., Twohy, C. H., Rogers, D. C., Baumgardner, D., Prenni, A. J.,

ACPD
13, 8701–8767, 2013

Campos, T., Gao, R., Anderson, J., and Feng, Y.: An overview of aircraft observations from the Pacific Dust Experiment campaign, J. Geophys. Res.-Atmos., 114, D05207, doi:10.1029/2008jd010924, 2009.
Streets, D. G., Fu, J. S., Jang, C. J., Hao, J., He, K., Tang, X., Zhang, Y., Wang, Z., Li, Z., Zhang, Q., Wang, L., Wang, B., and Yu, C.: Air quality during the 2008 Beijing Olympic Games, Atmos. Environ., 41, 480–492, doi:10.1016/j.atmosenv.2006.08.046, 2007.
Sullivan, R. C. and Prather, K. A.: Investigations of the diurnal cycle and mixing state of oxalic acid in individual particles in Asian aerosol outflow, Environ. Sci. Tech., 41, 8062–8069, doi:10.1021/es071134g, 2007.
Sullivan, R. C., Thornberry, T., and Abbatt, J. P. D.: Ozone decomposition kinetics on alumina: effects of ozone partial pressure, relative humidity and repeated oxidation cycles, Atmos. Chem. Phys., 4, 1301–1310, doi:10.5194/acp-4-1301-2004, 2004.
Sullivan, R. C., Guazzotti, S. A., Sodeman, D. A., and Prather, K. A.: Direct observations of the atmospheric processing of Asian mineral dust, Atmos. Chem. Phys., 7, 1213–1236, doi:10.5194/acp-7-1213-2007, 2007a.
Sullivan, R. C., Guazzotti, S. A., Sodeman, D. A., Tang, Y. H., Carmichael, G. R., and Prather, K. A.: Mineral dust is a sink for chlorine in the marine boundary layer, Atmos. Environ., 41, 7166–7179, doi:10.1016/j.atmosenv.2007.05.047, 2007b.
Sullivan, R. C., Minambres, L., DeMott, P. J., Prenni, A. J., Carrico, C. M., Levin, E. J. T., and Kreidenweis, S. M.: Chemical processing does not always impair heterogeneous ice nucleation of mineral dust particles, Geophys. Res. Lett., 37, L24805, doi:10.1029/2010gl045540, 2010a.
Sullivan, R. C., Petters, M. D., DeMott, P. J., Kreidenweis, S. M., Wex, H., Niedermeier, D., Hartmann, S., Clauss, T., Stratmann, F., Reitz, P., Schneider, J., and Sierau, B.: Irreversible loss of ice nucleation active sites in mineral dust particles caused by sulphuric acid condensation, Atmos. Chem. Phys., 10, 11471–11487, doi:10.5194/acp-10-11471-2010, 2010b.
Twohy, C. H. and Poellot, M. R.: Chemical characteristics of ice residual nuclei in anvil cirrus clouds: evidence for homogeneous and heterogeneous ice formation, Atmos. Chem. Phys., 5, 2289–2297, doi:10.5194/acp-5-2289-2005, 2005.
Usher, C. R., Michel, A. E., and Grassian, V. H.: Reactions on mineral dust, Chem. Rev., 103, 4883–4939, doi:10.1021/cr020657y, 2003a.
Usher, C. R., Michel, A. E., Stec, D., and Grassian, V. H.: Laboratory studies of ozone uptake on processed mineral dust, Atmos. Environ., 37, 5337–5347, 2003b.

ACPD
13, 8701–8767, 2013

Vali, G.: Nucleation terminology, B. Am. Meteorol. Soc., 66, 1426–1427, 1985.
Vlasenko, A., Sjogren, S., Weingartner, E., Gaggeler, H. W., and Ammann, M.: Generation of submicron Arizona test dust aerosol: chemical and hygroscopic properties, Aerosol Sci. Tech., 39, 452–460, doi:10.1080/027868290959870, 2005.
Wagner, C., Hanisch, F., Holmes, N., de Coninck, H., Schuster, G., and Crowley, J. N.: The interaction of N_2O_5 with mineral dust: aerosol flow tube and Knudsen reactor studies, Atmos. Chem. Phys., 8, 91–109, doi:10.5194/acp-8-91-2008, 2008.
Wang, B. B., Laskin, A., Roedel, T., Gilles, M. K., Moffet, R. C., Tivanski, A. V., and Knopf, D. A.: Heterogeneous ice nucleation and water uptake by field-collected atmospheric particles below 273 K, J. Geophys. Res.-Atmos., 117, D00v19, doi:10.1029/2012jd017446, 2012.
Welti, A., Lüönd, F., Stetzer, O., and Lohmann, U.: Influence of particle size on the ice nucleating ability of mineral dusts, Atmos. Chem. Phys., 9, 6705–6715, doi:10.5194/acp-9-6705-2009, 2009.
Welti, A., Lüönd, F., Kanji, Z. A., Stetzer, O., and Lohmann, U.: Time dependence of immersion freezing: an experimental study on size selected kaolinite particles, Atmos. Chem. Phys., 12, 9893–9907, doi:10.5194/acp-12-9893-2012, 2012.
Wheeler, M. J. and Bertram, A. K.: Deposition nucleation on mineral dust particles: a case against classical nucleation theory with the assumption of a single contact angle, Atmos. Chem. Phys., 12, 1189–1201, doi:10.5194/acp-12-1189-2012, 2012.
Yin, X. and Miller, J. D.: Wettability of kaolinite basal planes based on surface force measurements using atomic force microscopy, Miner. Metall. Proc., 29, 13–19, 2012.
Zettlemoyer, A. C., Tcheurekdjian, N., and Chessick, J. J.: Surface properties of silver iodide, Nature, 192, 653–653, 1961.
Zimmermann, F., Ebert, M., Worringen, A., Schutz, L., and Weinbruch, S.: Environmental scanning electron microscopy (ESEM) as a new technique to determine the ice nucleation capability of individual atmospheric aerosol particles, Atmos. Environ., 41, 8219–8227, doi:10.1016/j.atmosenv.2007.06.023, 2007.
Zipser, E. J., Twohy, C. H., Tsay, S.-C., Hsu, N. C., Heymsfield, G. M., Thornhill, K. L., Tanelli, S., Ross, R., Krishnamurti, T. N., Ji, Q., Jenkins, G., Ismail, S., Ferrare, R., Chen, G., Browell, E. V., Anderson, B., Hood, R., Goodman, H. M., Heymsfield, A., Halverson, J., Dunion, J. P., Douglas, M., and Cifelli, R.: The Saharan air layer and the fate of African easterly waves – NASA's AMMA field study of tropical cyclogenesis, B. Am. Meteorol. Soc., 90, 1137–1156, doi:10.1175/2009bams2728.1, 2009.

ACPD
13, 8701–8767, 2013

Table 1. List of kinetic variables calculated from O_3 ageing of MD particles. Ozone concentrations indicated in the first column are initial concentrations immediately before introducing aerosol into the tank but after accounting for background wall loss.

Particle and $[O_3]$ (ppbv)	1st order rate constant (k_{obs} min^{-1})	C_{mass} (g m^{-3})	Active Surface Site Coverage (molec cm^{-2})	Average Uptake (γ)
Ka + 425	$(1.42 \pm 0.13) \times 10^{-2}$	2.9×10^{-3}	$(6.5 \pm 1.0) \times 10^{15}$	$(7.1 \pm 1.1) \times 10^{-5}$
Ka + 427	$(1.16 \pm 0.05) \times 10^{-2}$	3.4×10^{-3}	$(6.0 \pm 1.0) \times 10^{15}$	$(4.9 \pm 0.6) \times 10^{-5}$
Ka + 430	$(1.02 \pm 0.05) \times 10^{-2}$	3.4×10^{-3}	$(5.5 \pm 0.9) \times 10^{15}$	$(4.3 \pm 0.6) \times 10^{-5}$
ATD + 433	$(0.44 \pm 0.02) \times 10^{-2}$	2.1×10^{-4}	$(5.0 \pm 0.8) \times 10^{16}$	$(6.3 \pm 0.6) \times 10^{-4}$
ATD + 425	$(0.40 \pm 0.05) \times 10^{-2}$	5.3×10^{-4}	$(1.6 \pm 0.3) \times 10^{16}$	$(2.3 \pm 0.4) \times 10^{-4}$

ACPD
13, 8701–8767, 2013

Table 2. Metrics to compare immersion freezing efficiency of Ka and ATD particles.

Particle Type ([O_3])	$T_{50\%} \pm 0.4$ K	$T_{onset} \pm 0.4$ K
Ka – Low Exposure (427 ppbv)	239.5	252.0
Ka – Untreated	238.0	245.5
Ka – High Exposure (1.4 ppmv)	236.0	244.0
ATD – Low Exposure (429 ppbv)	244.1	260.0
ATD – Untreated	243.6	260.5
ATD – High Exposure (4.3 ppmv)	240.5	260.9

ACPD
13, 8701–8767, 2013

Table 3. Fits for deposition mode ice active fraction as a function of temperature (K) at $RH_w = 95\,\%$ as shown in Fig. 8.

O_3 exposure level	Ka	ATD
None	$AF = e^{(79.0-0.36T)}$	$AF = e^{(65.3-0.30T)}$
Low	$AF = e^{(81.7-0.36T)}$	$AF = e^{(51.8-0.25T)}$
High	N/A	$AF = e^{(66.4-0.31T)}$

ACPD
13, 8701–8767, 2013

Table 4. Fits for immersion mode ice active fraction as a function of temperature (K) as shown in Fig. 9.

O_3 exposure level	Ka	ATD
None	$AF = 0.012 + \left[\frac{0.988}{1+10^{-0.303(238.0-T)}}\right]$	$AF = 0.044 + \left[\frac{0.956}{1+10^{-0.168(243.3-T)}}\right]$
Low	$AF = 0.045 + \left[\frac{0.955}{1+10^{-0.395(239.5-T)}}\right]$	$AF = 0.046 + \left[\frac{0.954}{1+10^{-0.191(244.0-T)}}\right]$
High	$AF = 0.103 + \left[\frac{0.897}{1+10^{-0.293(236.7-T)}}\right]$	$AF = 0.048 + \left[\frac{0.952}{1+10^{-0.157(240.2-T)}}\right]$

ACPD
13, 8701–8767, 2013

Table 5. Fits for deposition mode ice active surface site density (m^{-2}) as a function of temperature (K) at $RH_w = 95\,\%$ as shown in Fig. 10.

O_3 exposure level	Ka	ATD
None	$n_s = e^{(115.17212-0.3952T)}$	$n_s = e^{(98.44267-0.31858T)}$
Low	$n_s = e^{(107.54728-0.3561T)}$	$n_s = e^{(94.33849-0.30282T)}$
High	N/A	$n_s = e^{(102.21129-0.3418T)}$

ACPD
13, 8701–8767, 2013

Table 6. Fits for immersion mode ice active surface site density (m^{-2}) as a function of temperature (K) as shown in Fig. 11.

O_3 exposure level	Ka	ATD
None	$n_s = e^{(116.3-038T)}$	$n_s = e^{(79.4-0.21T)}$
Low	$n_s = e^{(101.7-0.31T)}$	$n_s = e^{(70.5-0.17T)}$
High	$n_s = e^{(94.7-0.29T)}$	$n_s = e^{(100.2-0.30T)}$

ACPD
13, 8701–8767, 2013

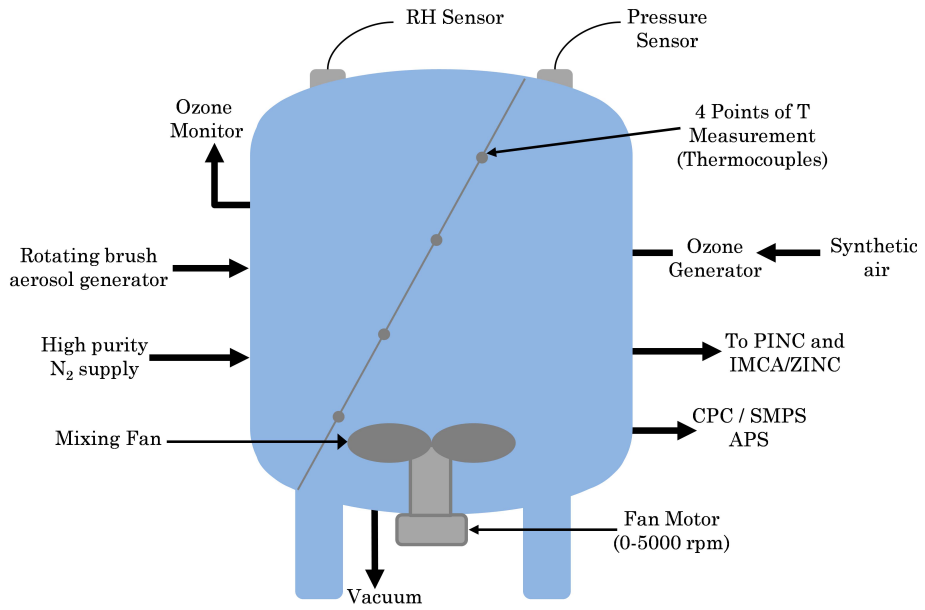

Fig. 1. Schematic of the experimental set up around the stainless steel aerosol tank. The diameter and height dimensions given in the text for the tank are taken at the centre of the tank, these are not uniform since the tank has curved edges. In addition two features not used in the current work are not shown in the figure, the large connector ports (4 × CF40).

ACPD
13, 8701–8767, 2013

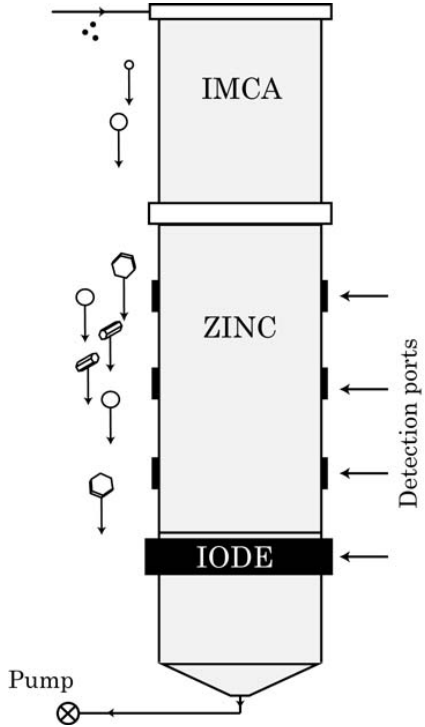

Fig. 2. Front view schematic of the immersion freezing experimental set up (*modified from* Welti et al., 2012). The top part of the chamber is used to activate droplets followed by freezing in the lower part. The position of IODE as indicated in the schematic corresponds to the 12 s residence time in ZINC for a total flow rate of 10 L min^{-1} (see text). The detector can be mounted on different ports so as to study time dependence of immersion freezing (Welti et al., 2012).

ACPD
13, 8701–8767, 2013

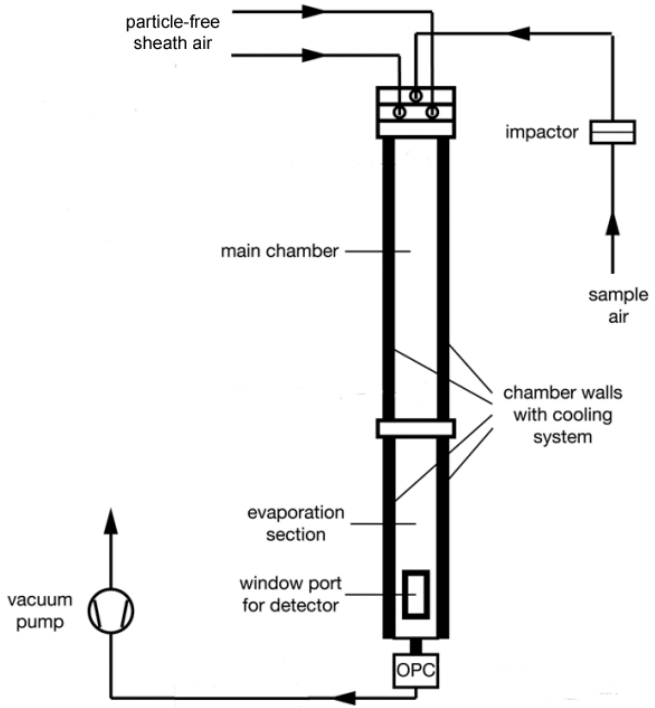

Fig. 3. Schematic of the cross section of the Portable Ice Nucleation Chamber (PINC) used for deposition mode experiments in this work. Chamber walls coated with ice are shown as bold lines. An extra window port also allows the option to mount IODE onto PINC (not done in the current work).

ACPD
13, 8701–8767, 2013

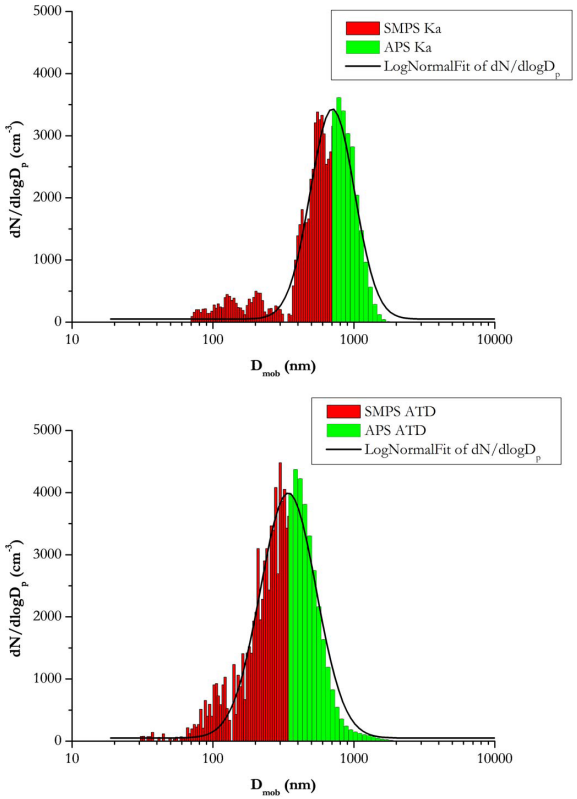

Fig. 4. Representative number size distributions for Ka (top) and ATD (bottom) of suspended dust particles in aerosol tank recorded with an SMPS and APS simultaneously. We note that IN counters sampled through a 1 µm impactor necessitating the use of particle number distributions of less than 1.14 µm aerodynamic diameter for ice active fraction calculations.

ACPD
13, 8701–8767, 2013

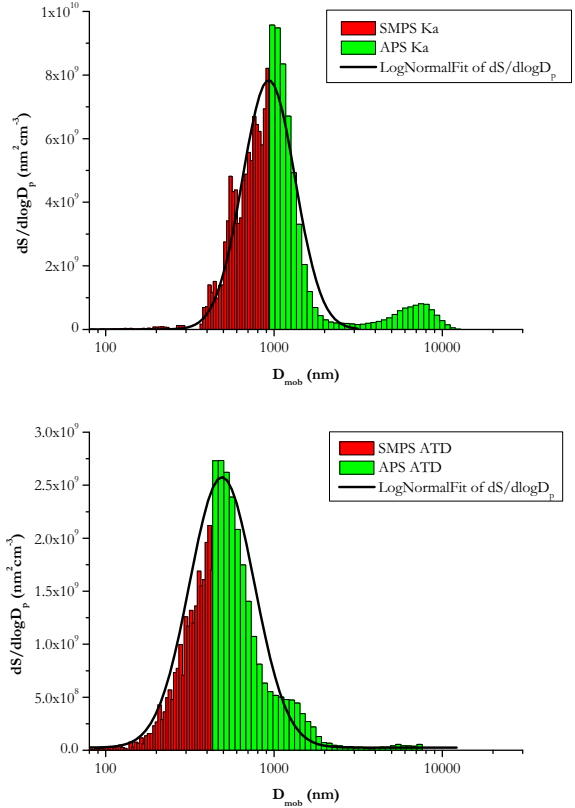

Fig. 5. Representative surface area distributions for Ka (top) and ATD (bottom) of suspended dust particles in aerosol tank recorded with an SMPS and APS simultaneously. We note that IN counters sampled through a 1 µm impactor necessitating the use of surface distributions of less than 1.14 µm aerodynamic diameters for IASSD calculations.

ACPD
13, 8701–8767, 2013

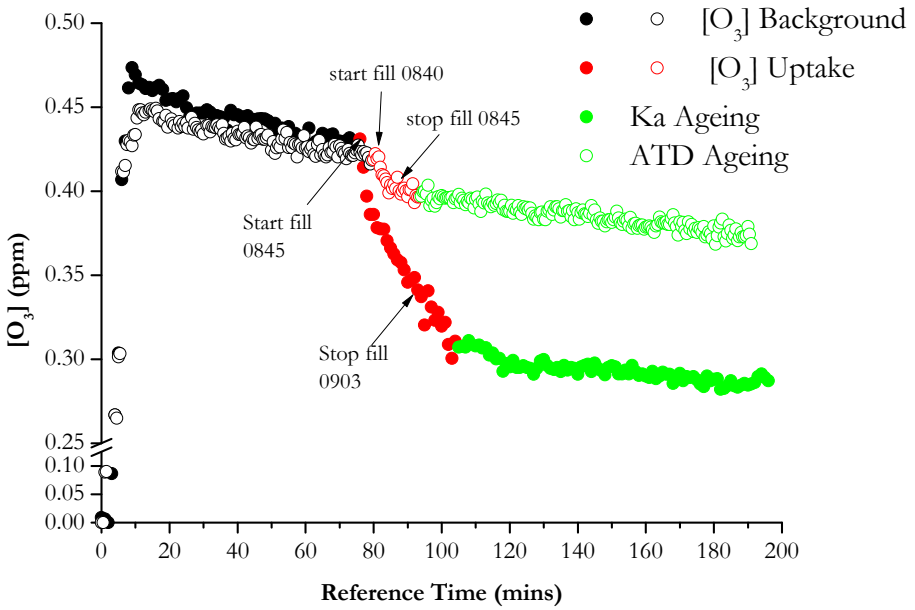

Fig. 6. Time series for O_3 ageing experiments in the aerosol tank. O_3 is added to the tank and a background wall-loss rate is observed. Then mineral dust particles are added to the tank increasing the loss rates. This uptake rapidly relaxes to background levels after or shortly after the addition of dust to the tank has been terminated. Arrows on the graph indicated start and stop times for filling dust. O_3 loss to the particle surface was considered to be first order.

ACPD
13, 8701–8767, 2013

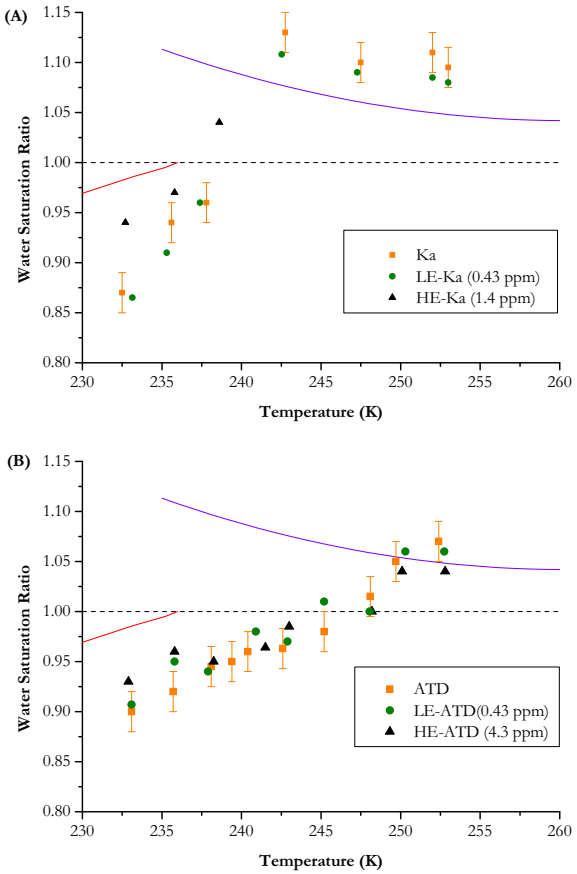

Fig. 7. Ice activated fraction for 0.1 % of the particle population forming ice as a function of temperature in the deposition mode **(A)** Ka and **(B)** ATD. Dashed line: $RH_w = 100\,\%$, red line: freezing of 0.1 % 300 nm ammonium sulphate particles in 10 s (Koop et al., 2000; DeMott et al., 2009), purple line: water drop survival line for PINC.

ACPD
13, 8701–8767, 2013

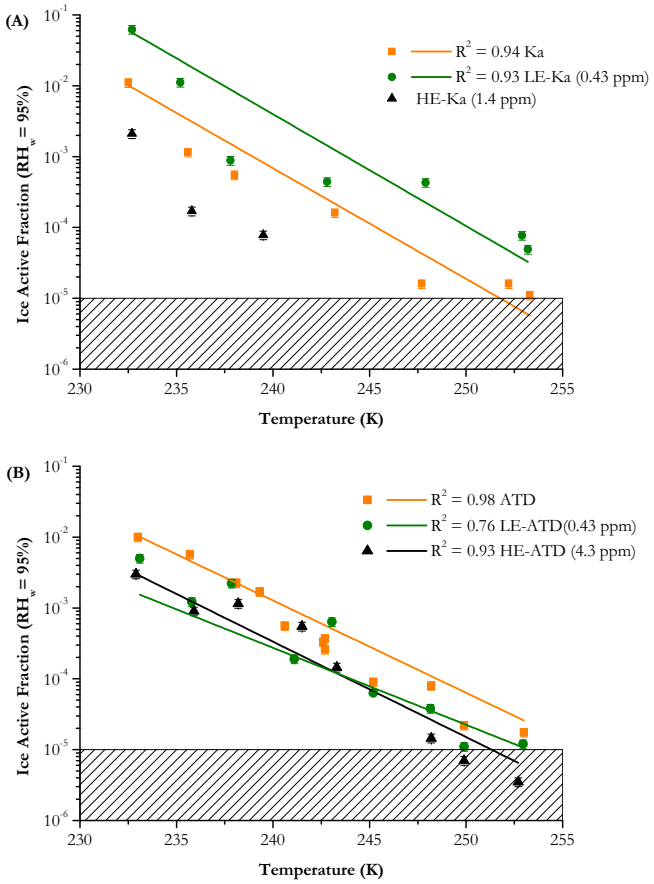

Fig. 8. Ice activated fraction at RH_w = 95 % as a function of temperature for deposition mode nucleation of **(A)** Ka and **(B)** ATD. Exponential fit equations for curves are presented in Table 3. Hashed region represents instrument detection limit for PINC. A fit for the HE-Ka was not calculated obtained because of the few data points collected.

ACPD
13, 8701–8767, 2013

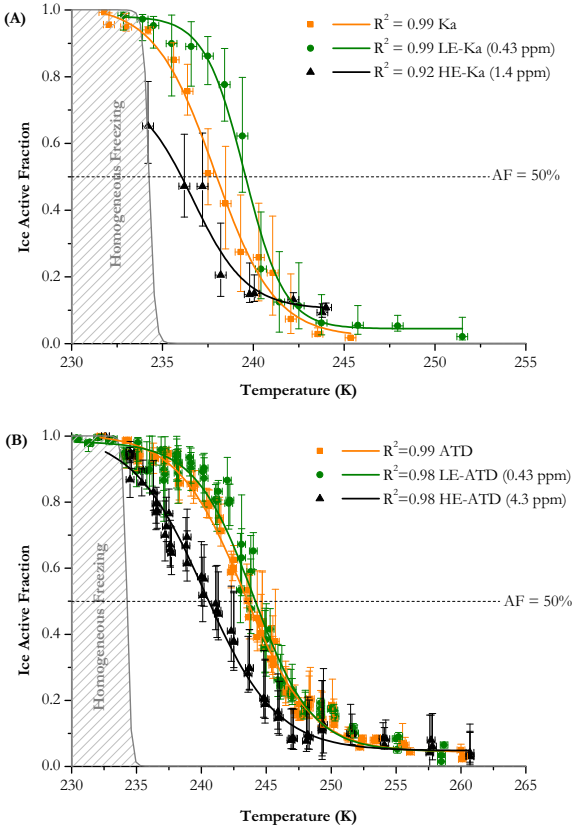

Fig. 9. Ice activated fraction as a function of temperature for immersion mode nucleation of **(A)** Ka and **(B)** ATD. Homogeneous freezing parameterisation is for 10 µm water droplets (Earle et al., 2010). Dashed line indicates 50 % of particles frozen. The temperature at which this line intersects the fit lines refers to $T_{50\%}$ (see text for more details).

ACPD
13, 8701–8767, 2013

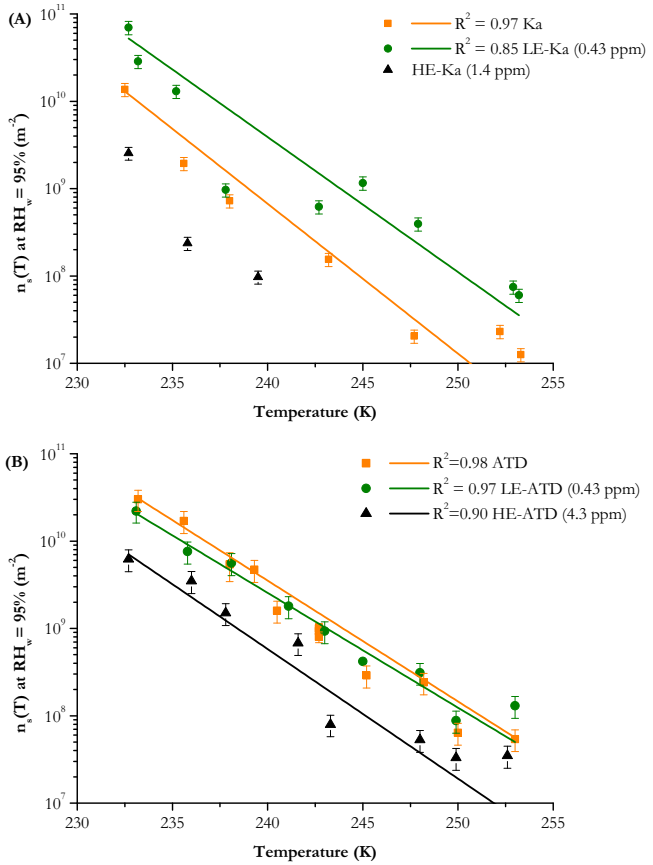

Fig. 10. Ice active surface site densities as a function of temperature for deposition mode at RH_w = 95 % **(A)** Ka and **(B)** ATD. Exponential fit functions to data are presented in Table 5.

ACPD
13, 8701–8767, 2013

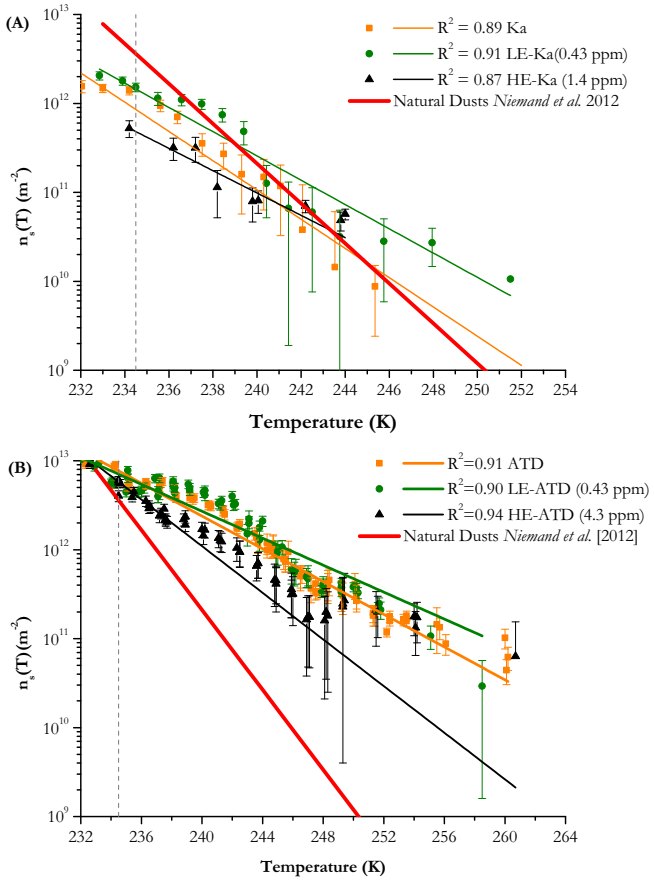

Fig. 11. Ice active surface site densities as a function of temperature for immersion mode freezing of **(A)** Ka and **(B)** ATD. Exponential fit functions to data are given in Table 6. Dashed line: homogeneous freezing temperature for 10 µm water droplets (Earle et al., 2010). Fit function for natural dusts from Niemand et al. (2012): $n_s(T) = \exp(-0.517T + 8.934)$ (m^{-2}).

ACPD
13, 8701–8767, 2013